HHS Public Access

Author manuscript

Nanoscale. Author manuscript; available in PMC 2024 February 13.

Published in final edited form as:

Nanoscale. 2019 June 06; 11(22): 10791–10807. doi:10.1039/c9nr00807a.

Catalytic Oxidation and Reduction Reactions of Hydrophilic Carbon Clusters with NADH and Cytochrome C: Features of an Electron Transport Nanozyme

Paul J. Derry[⁂,‡], **Lizanne G. Nilewski**[※], **William K. A. Sikkema**[※], **Kimberly Mendoza**[※], **Almaz Jalilov**[^], **Vladimir Berka**[‼], **Emily A. McHugh**[※], **Ah-Lim Tsai**[‼], **James M. Tour**[*,※,§,±], **Thomas A. Kent**[*,⁂,⁜,※]

[⁂] -Texas A&M Health Science Center Institute of Biosciences and Technology, Houston, Texas 77030, United States

[‡] -Neurology and Center for Translational Research in Inflammatory Diseases, Michel E. DeBakey VA Medical Center, Houston, Texas 77030, United States

[※] -Department of Chemistry, Rice University, 6100 Main Street, Houston, Texas 77005, United States

[§] -The NanoCarbon Center, Rice University, 6100 Main Street, Houston, Texas 77005, United States

[±] -Department of Materials Science and NanoEngineering, Rice University, 6100 Main Street, Houston, Texas 77005, United States

[^] -Department of Chemistry and Center for Integrative Petroleum Research, King Fahd University of Petroleum and Minerals, Dhahran, Saudi Arabia, 31261

[‼] -Hematology, Internal Medicine, University of Texas Houston Medical School, Houston, Texas 77030, United States

[⁜] -Stanley H. Appel Department of Neurology, Houston Methodist Hospital and Institute of Academic Medicine, Houston, Texas 77030, United States

Abstract

Previously, our group reported on the promising efficacy of poly(ethylene glycol)-hydrophilic carbon clusters (PEG-HCCs) to work as broadly active and high capacity antioxidants in brain ischemia and injury models including stroke and traumatic brain injury coupled with hemorrhagic shock. PEG-HCCs are a carbon nanomaterial derived from harsh oxidation of single wall carbon nanotubes and covalently modified with poly(ethylene glycol). They retain no tubular remnants and are composed of a highly oxidized carbon core functionalized with peroxyl, quinone, ketone, carboxylate, and hydroxyl groups. HCCs are the redox active carbon core of PEG-HCCs, which

[*]**Corresponding Author:** Thomas A. Kent, M.D. tkent@tamhsc.edu, James M. Tour, Ph.D. tour@rice.edu.

Disclosures

Drs. Kent and Tour are named inventors on intellectual property surrounding the PEG-HCCs, but that property is owned by Rice University, and in part by Baylor College of Medicine. That intellectual property is being licensed to a company in which JMT is a stockholder but not an officer or director. Conflicts of interest for JMT and TAK are managed through regular disclosures to their respective Office of Sponsored Programs and Research Compliance.

have a broad reduction potential range starting at +200 mV and extending to −2 V. Here we describe a new property of these materials: the ability to catalytically transfer electrons between key surrogates and proteins of the mitochondrial electron transport complex in a catalytic fashion consistent with the concept of a nanozyme. The estimated reduction potential of PEG-HCCs is similar to that of ubiquinone and they enabled the catalytic transfer of electrons from low reduction potential species to higher reduction electron transport complex constituents. PEG-HCCs accelerated the reduction of resazurin (a test indicator of mitochondrial viability) and cytochrome c by NADH and ascorbic acid in solution. Kinetic experiments suggested a transient tertiary complex. Electron paramagnetic resonance demonstrated NADH increased the magnitude of PEG-HCCs' intrinsic radical, which then reduced upon subsequent addition of cytochrome c or resazurin. Deconvolution microscopy identified PEG-HCCs in close proximity to mitochondria after brief incubation with cultured SHSY-5Y human neuroblastoma cells. Compared to methylene blue (MB), considered a prototypical small molecule electron transport shuttle, PEG-HCCs were more protective against toxic effects of hydrogen peroxide *in vitro* and did not demonstrate impaired cell viability as did MB. PEG-HCCs were protective *in vitro* when cells were exposed to sodium cyanide, a mitochondrial Complex IV poison. Because mitochondria are a major source of free radicals in pathology, we suggest that this newly described nanozyme action helps explain their *in vivo* efficacy in a range of injury models. These findings may also extend their use to mitochondrial disorders.

Keywords

Carbon nanomaterials; mitochondria; electron transport complex; redox chemistry; cyanide

Introduction

While some reactive oxygen species (ROS) serve as vital signaling molecules in cellular homeostasis,[1] ROS dysregulation is pervasive in the pathologies such as stroke, sepsis and traumatic brain injury (TBI).[2] Electron leakage, a process whereby reduced mitochondrial constituents are intercepted by unwanted oxidants not only reduces the efficiency of mitochondria, but also generates free radicals that can cause further damage. Electron leakage is a notable result of aging and pathologies such as TBI and focal ischemia reperfusion injury,[3, 4] which are caused by the return of dioxygen to electrochemically reduced tissue.[5] The reduced electron transport complex constituents, flavin mononucleotide ($FMNH_2$), nicotinamide adenine dinucleotide (phosphate) (NAD(P)H), ubiquinone (QH_2) and their enzymatic hosts, Complexes I, II,[6] and III, are principally associated with generating superoxide in mitochondria because they are chokepoints in the electron transport complex that can non-specifically donate electrons to dioxygen, reducing electron transport complex efficiency. Ideally, a drug that could bypass an inhibited mitochondrial Complex, or transport electrons to higher reduction potential mitochondrial constituents could help to alleviate electron leakage and the damaging ROS that result.

Previously, our group reported on the promising efficacy of poly(ethylene glycol)-hydrophilic carbon clusters (PEG-HCCs) in both oxidative injury and delayed-treatment reperfusion models, without any evidence of acute toxicity, or injury after 6 weeks, in

normal mice.[4, 7–10] PEG-HCCs are a type of oxidized graphene nanoribbon composed of a highly oxidized carbon core with peroxyl, quinone, ketone, carboxylate, and hydroxyl functional groups.[8, 11, 12] The redox chemistry of PEG-HCCs has been explored and it showed that they catalytically dismutate superoxide ($O_2^{\bullet-}$) into hydrogen peroxide (H_2O_2) and dioxygen (O_2), and PEG-HCCs effectively quench hydroxyl radical (•OH).[11, 12] *In vivo* effects showed a restoration of oxidative balance between superoxide and nitric oxide, a dramatic reduction in tissue death and maintenance of blood flow following ischemia by cerebral impact complicated by hemorrhagic shock in rats.[4, 10]

The versatility, functionality and lack of toxicity thus far of PEG-HCCs make them attractive candidates for clinical translation. Their broad effectiveness suggests that their mechanism of action may not solely be limited to superoxide and hydroxyl radical quenching, especially given the disappointing results of other antioxidants.[11] This hypothesis is supported by our previous work demonstrating that PEG-HCCs protected bEnd.3 cells from toxicity associated with antimycin A (AntA); while AntA instigates the generation of superoxide in mitochondria, it is primarily an electron transport complex inhibitor.[4] Later, we demonstrated that PEG-HCCs were capable of oxidizing ascorbic acid.[7] Consistent with these prior findings, we sought to determine if PEG-HCCs could participate in other biochemically relevant pathways specifically as catalytic electron transfer in conditions relevant to disruption of mitochondrial oxidative phosphorylation. Our findings suggest that indeed these materials are able to catalyze several reactions relevant to mitochondria function, features consistent with the concept of a nanomaterial with enzymatic properties, or nanozyme.[13]

Electron shuttles are crucial in cellular respiration (Fig. 1). Since components of the electron transport complex are spatially separated in the inner membrane of mitochondria, small carrier molecules are needed to facilitate the transfer of electrons. For instance, ubiquinone has a standard reduction potential near 40–50 mV and transports electrons from Complex I to Complex III. Ferricytochrome c ($CytC_{ox}$) has a standard reduction potential of +250 mV, a value between the reduction potentials of cytochrome c_1 (+220 mV, Complex III reductase subunit) and cytochrome a (+290 mV, Complex IV oxidase subunit) (Fig. 1).

Analogously, there is a body of work regarding methylene blue (MB)) as a potential electron transport shuttle (ETS). Atamna *et al.* and Lee *et al.* showed that MB was capable of functioning as an electron transport shuttle (ETS) by oxidizing low reduction potential species and reducing high reduction potential species in the electron transport complex.[14, 15] MB has shown other effects such as inhibition of xanthine oxidase which secondarily reduces intracellular superoxide production.[16] In this report, we describe our work on characterizing the catalytic activity of PEG-HCCs with respect to NADH and ascorbic acid as electron donors and resazurin and CytC as electron recipients using UV-vis spectrophotometry.

We also wanted to determine if SOD mimicry by a graphene-like small molecule was related to catalytic electron transfer so we compared the cell free system activity of the aromatic small molecule, poly(ethylene glycol)-functionalized perylene diimide, which

possess comparable superoxide dismutase mimetic activity,[17] to PEG-HCCs in order to assess whether SOD mimetic activity is separable from the shuttling effect we report herein.

Deconvolution microscopy was performed of cells cultured with PEG-HCCs to detect co-localization between PEG-HCCs and mitochondria. Comparison of PEG-HCCs to MB both as a function of their reaction kinetics and in a H_2O_2 protection assay was performed. Lastly, we tested *in vitro* their potential therapeutic application as an antidote for the mitochondrial poison cyanide.

Results

Cyclic Voltammetry of PEG-HCCs

Cyclic voltammograms of PEG-HCCs adsorbed to glassy carbon electrodes in phosphate buffered saline (PBS) demonstrated that PEG-HCCs have a broad pattern with reduction maxima at 2 negative potentials (Fig. 2). The cyclic voltammogram of the glassy carbon electrodes is shown in Supplemental Fig. 1 and shows no response up to −1800 mV. The first reduction occurs at approximately −750 mV and the second reduction occurs at approximately −1750 mV. The first reduction extends from +200 mV to −1250 mV and suggests that PEG-HCCs could be reduced by species with reduction potentials less than 0 V. Due to the solubility of PEG-HCCs in PBS, and the small amount of adsorbed material it was not possible to reliably obtain multiple scans in the sample to find electrochemical reversibility. At voltages above +200 mV the particles appear to begin to oxidize, however at voltages greater than +500 mV we are unable to distinguish sample oxidation current from background capacitive current from buffer oxidation.

Catalytic Reduction of Resazurin and CytC by PEG-HCCs

Using resazurin as an electron acceptor and indicator of reaction progression, reaction rates were collected for the reduction of resazurin by NADH in the presence of PEG-HCCs using a spectrophotometric plate reader with samples prepared in triplicate (Fig. 3). By increasing the concentration of PEG-HCCs, the reaction rate increased linearly as the concentration was varied from 0 mg/L to 32 mg/L. Solutions containing PEG-HCCs formed resorufin faster than without (1.8×10^{-10} M/s), consistent with PEG-HCCs acting as a catalyst towards the reduction of resazurin by NADH (Fig. 3A). Varying the concentration of NADH while fixing the concentration of PEG-HCCs (4 mg/L) and resazurin (40 μM) resulted in the reaction rate increasing linearly within a range of NADH from 0 mM to 0.5 mM. Because the reaction rate was 1.8×10^{-10} M/s when NADH was not present in the solution and was linearly dependent upon the concentration of NADH, we conclude that NADH was the source of the electrons and not the result of resazurin-induced oxidation of the PEG-HCCs.

The concentration of resazurin was varied from 3.75 μM to 125 μM at three different concentrations of NADH, 2 mM, 1 mM and 0.5 mM. The resulting curves (Fig. 3C) resembled saturation curves like those found in enzymes and suggested that PEG-HCCs were saturable catalysts with respect to the reduction of resazurin, making the use of Michaelis-Menten reaction kinetics a reasonable choice to characterize the particles. The

kinetic parameters V_{max}, K_M and k_{cat} were calculated for the reaction between NADH, PEG-HCCs and resazurin as shown in Table 1.

Next, the reaction kinetics curves were transformed using a Lineweaver-Burk double reciprocal (Fig. 3D) and generated three intersecting lines where the slope of the lines decreased as the concentration of NADH increased, consistent with a ternary complex (a transient state consisting of both substrates adsorbed to the catalyst[18]) during the reaction between NADH, PEG-HCCs and resazurin.

The reaction kinetics between NADH, PEG-HCCs and $CytC_{ox}$ were studied due to the important role that $CytC_{ox}$ plays in the electron transport complex and to determine if it were chemically feasible for PEG-HCCs to serve as an electron shuttle in the mitochondrial electron transport complex between NADH and $CytC_{ox}$. Using the same methodology as was done with resazurin, the concentration of NADH was varied between 0.5 and 2 mM and the concentration of $CytC_{ox}$ was varied from 3.75 μM to 125 μM. The resulting curves were sigmoidal which suggested a cooperative effect in the interaction of $CytC_{ox}$ with PEG-HCCs in this reaction (Fig. 3E).[19] The rate of reduction without PEG-HCCs is shown in Supplemental Fig. 2 indicating that without PEG-HCCs, the reaction between NADH and $CytC_{ox}$ is much slower. Because the curves were not hyperbolic but were sigmoidal, we chose to use the Allosteric Sigmoidal curve fitting model in Prism Graphpad 8 to obtain the kinetic parameters, V_{max}, h, and K_{half}.[20, 21] The kinetics parameters for the reaction between NADH, PEG-HCCs, and CytC are shown in Table 2. The results show that the reduction of $CytC_{ox}$ by NADH is catalyzed by PEG-HCCs and that the Hill coefficient, a measure of cooperativity (h),[19] is greater than 2, indicating a positively cooperative effect with respect to $CytC_{ox}$ concentration.[20]

Additionally, the reaction may be saturable above a certain concentration of NADH as the V_{max} for the highest concentration of NADH tested, 2 mM, is not double the V_{max} for 1 mM, or four times the rate for 0.5 mM NADH.

The reactivity of PEG-HCCs with resazurin and ascorbic acid (Asc) was investigated. Asc is a vital antioxidant and is used by mitochondria to protect against oxidative stress caused by aerobic respiration.[22] We have previously shown that ascorbic acid can be oxidized by 20 mg/L PEG-HCCs.[7] Because PEG-HCCs can oxidize Asc, we hypothesized that Asc could be an electron source for the electron transport capabilities of PEG-HCCs. To test the potential role of ascorbate as an electron source for PEG-HCCs, the reduction kinetics experiments were repeated with Asc as the reductant instead of NADH (Fig. 4A). A concentration range from 250 μM to 62.5 μM Asc was used instead of the 2 mM – 0.5 mM range with NADH because the reaction with Asc was too fast to accurately measure without increasing the sampling rate and thus the amount of light the sample was exposed to.

The reaction rates were fit to hyperbolic Michaelis-Menten saturation curves the V_{max}, K_M and k_{cat} parameters were obtained for the three different concentrations of Asc (Table 3). The V_{max} for the highest concentration of Asc tested, 250 μM, was nearly 3-fold higher than the V_{max} for the highest concentration of NADH, 2 mM, 5.8×10^{-9} M/s vs 1.9×10^{-8} M/s for NADH and Asc respectively. The K_M for both NADH and Asc were within the same order

of magnitude, however the k_{cat} parameters were one order of magnitude apart. PEG-HCCs have a higher k_{cat} in the presence of Asc than they do NADH, 0.75 vs 0.06 s^{-1}, respectively.

Transforming the Michaelis-Menten plots of Asc with PEG-HCCs and resazurin showed that the resulting lines intersected suggesting again that a ternary complex formed in this reaction (Fig. 4B).[18]

Electron Paramagnetic Resonance of PEG-HCCs with NADH and Resazurin and CytC

To help understand the reaction mechanism between PEG-HCCs, NADH, resazurin, and, ferricytochrome c ($CytC_{ox}$), the effects of NADH, resazurin, and cytochrome $CytC_{ox}$ on PEG-HCCs were studied using electron paramagnetic resonance (EPR). PEG-HCCs have an intrinsic radical, as we reported in Samuel *et al.*,[23] that is sensitive to changes in electron density and radical state.[24] To understand the role of PEG-HCCs in this reaction, EPR studies were performed with NADH, and the oxidizer ($CytC_{ox}$ or resazurin), and with only the oxidizer. In the first experiment, a solution of PEG-HCCs (400 mg/L, 2.5 μM) and NADH (300 μM) was prepared and the intrinsic radical measured. It was found that the intensity of the PEG-HCCs' intrinsic radical increased in the presence of NADH by 30–40% after 10 min (Fig. 5A). The addition of $CytC_{ox}$ (150 μM) or resazurin (150 μM) to the solution of PEG-HCCs and NADH resulted in a reduction in the intrinsic radical signal intensity to slightly below the baseline intensity (Fig. 5B) within 10 s. The increase in the intrinsic radical intensity of PEG-HCCs by NADH is time-dependent and gives an approximately 30–40% increase in signal intensity after 5 min (Fig. 5C, 5D). When PEG-HCCs were treated with resazurin, no effect on the intrinsic radical was observed. However, a slight increase was observed after the addition of $CytC_{ox}$ (Supplemental Figure 3).

Stoichiometry of PEG-HCC catalyzed reduction of $CytC_{ox}$ by NADH

UV-vis spectroscopy of solutions containing PEG-HCCs, $CytC_{ox}$ and NADH were performed to determine the molar ratio of NADH to $CytC_{ox}$ consumed in this catalyzed reaction. This was performed by measuring the absorbance of the 340 nm peak (associated with NADH) and the absorbance of the 550 nm peak (associated with $CytC_{red}$) at 0 and 30 min, finding the difference and dividing the difference in absorbance by the respective extinction coefficients (6.22 mM^{-1} cm^{-1} for NADH, and 21.84 mM^{-1} cm^{-1} for $CytC_{red}$).[25, 26] After adjusting for molar extinction coefficients, it was found that $CytC_{red}$ was formed at a rate nearly two-fold faster than NADH was oxidized.

Effect of Ethylenediamine-functionalization on PEG-HCCs

Ethylenediamine-functionalized PEG-HCCs (EN-PEG-HCCs) were synthesized by reacting PEG-HCCs with ethylenediamine at room temperature in order to convert quinone residues to imines so as to functionally eliminate their contribution.[27] Cyclic voltammetry showed that the reduction maxima at −750 mV had disappeared in the EN-PEG-HCCs (Fig. 6A). A weak shoulder appeared at approximately −1500 mV in the EN-PEG-HCCs. The reaction rates of 4 mg/L PEG-HCCs were compared to 4 mg/L EN-PEG-HCCs and it was found that within the resazurin concentration range tested the EN-PEG-HCCs did not exhibit saturation

kinetics and that the reaction rates were approximately 50% of the PEG-HCCs at the highest concentration of resazurin tested (64 μM). (Fig. 6B).

In a single experiment, to determine if quinones contributed to the protective effects of PEG-HCCs, we performed a hydrogen peroxide treatment assay in which PEG-HCCs are protective (see Figure 9 and Fabian *et al.*[10]). bEnd.3 cells were treated with 100 μM H_2O_2 followed immediately by EN-PEG-HCCs and incubated overnight. The following morning, the remaining live cells were counted. It was observed that 100 μM H_2O_2 reduced the number of live cells to 57% of the untreated control and no protection was afforded by addition of EN-PEG-HCCs (57% of control), while the EN-PEG-HCCs did not reduce viability (109% of control).

Comparison of Resazurin Reduction by PEG-HCCs and PEG-PDIs

PEG-PDIs are poly(ethylene glycol)-functionalized perylene diimides consisting of a highly conjugated perylene core with two PEG chains bound to the N-terminals of the perylene diimide group.[17] While they show excellent SOD-mimetic activity,[17] their CV reduction potential differs from the PEG-HCCs in that the reduction peak is narrow and centered at −460 mV vs. SCE (−216 mV vs. SHE).[28] The reaction rates of PEG-HCCs and PEG-PDIs within a concentration range of 4–32 mg/L in 0.5 mM NADH and 1.1 μM resazurin were compared and it was found that PEG-PDIs did not catalyze the reaction with resazurin and the reaction rate for all concentrations was essentially zero (Fig. 7).

Colocalization of PEG-HCCs with Mitochondria in Cultured Cells

We previously showed by transmission electron microscopy that PEG-HCCs were detected in the mitochondria after incubation with T-lymphocytes.[29] Here we employed deconvolution microscopy to better visualize the distribution within the cell. Deconvolution microscopy images of SHSY-5Y cells expressing green fluorescent protein (GFP, green) with a CytC oxidase subunit IV targeting sequence.[30] In the Z-projection shown in Fig. 8A, AlexaFluor-647 signal is localized inside and around the cell indicating the presence of PEG-HCCs. The upper and lower frames of the Z-stack were excluded because of optical defocusing. To determine if the PEG-HCCs were colocalized with the GFP signal, the GFP and AlexaFluor 647 signals on each layer within the Z-stack were binarized using ImageJ and a binary AND operation of the GFP and AlexaFluor 647 channels was performed (Fig. 8B) at each layer. Overlap of the GFP and AlexaFluor 647 signals was observed within each layer (yellow). The Z-projection of the binary AND of those overlapping areas shown in Fig. 8B shows a considerable number of overlapping signals. The location of those overlaps with respect to the labeled mitochondria are shown in Fig. 8C (Yellow on green).

The PEG-HCCs appeared to be closely associated with the membrane envelope of the cells (Fig. 8A), a behavior consistent with the amphiphilic characteristics of PEG-HCCs.[31] The PEG chains provide excellent water solubility, but the oxidized aromatic carbon core may be lipophilic and interact with the lipid rafts of the plasma membrane and mitochondrial outer membranes.[32] This localization in the membrane could also potentially contribute to cell protection against membrane lipid peroxidation, an important consequence of oxidative injury.[33, 34]

Comparison of PEG-HCC Reaction Kinetics with MB

MB is a prototypical electron shuttle with demonstrated clinical efficacy in treating methemoglobinemia by oxidizing NAD(P)H in erythrocytes to reduce methemoglobin to hemoglobin.[35] PEG-HCCs and MB are electrochemically similar with respect to midpoint potentials, or the $E_{1/2}$ of the oxidation-reduction cycle, of +11 mV and ~0 mV respectively, although PEG-HCCs have a much broader range.[12, 14] Based on the findings in this report, PEG-HCCs may have similar effects on the electron transport complex as described for MB.[36, 37] To make a more direct comparison of MB to PEG-HCCs, Michaelis-Menten parameters for MB were collected with respect to NADH and $CytC_{ox}$ using a fixed concentration of MB (4 mg/L, 12.5 μM) and NADH (500 μM). Because the size distribution of PEG-HCCs is not well-defined, we chose to directly compare identical mass concentrations of PEG-HCCs to MB.[8] Kinetics parameters V_{max}, h, and k_{half} were calculated for the reaction between NADH, MB and CytC (Table 4).

Compared to the previously collected data (Fig. 3E) with 500 μM NADH, the reaction with 4 mg/L MB had a V_{max} 7.7-fold higher than the reaction with 4 mg/L PEG-HCCs (20.22×10^{-9} M/s vs. 2.4×10^{-9} M/s, Fig. 9A). The hill coefficient (h) is greater than 2 for both MB (2.39) and PEG-HCCs (2.02) indicating a cooperative effect as CytC concentration is increased.[20] The K_{half}, or concentration of half-maximum velocity for MB is comparable to PEG-HCCs (5.21×10^{-6} M vs 4.8×10^{-6} M). Finally, the k_{cat} for PEG-HCCs was calculated to be 9.3×10^{-2}, roughly one order of magnitude higher than the k_{cat} for methylene blue (1.62×10^{-3})

To examine differential protective effects of these two agents, MB and PEG-HCCs were tested in a H_2O_2 challenge assay in cultured cells. H_2O_2 exerts toxic effects on endothelial cells through at least four routes: hydroxyl and superoxide radical formation by reacting with reduced species,[38] nitric oxide synthase (NOS) and NADPH oxidase (NOX) stimulation and uncoupling,[39] modulation of mitochondrial permeability,[40] and the Fenton reaction.[41] Our model employs administering the test agent after the H_2O_2 since efficacy under post-injury conditions would be critical for clinical translation for treatment following an injury, as we have discussed previously.[23]

PEG-HCCs and MB were compared in two standard H_2O_2 challenge assays (Fig. 9B–D). bEnd.3 murine cerebrovascular endothelial cells were treated with PEG-HCCs, and 100 μM H_2O_2 both with and without 8 mg/L PEG-HCCs. The PEG-HCC concentration was derived from prior experiments that also approximate the blood levels we estimate in our rodent models.[4, 7, 10] Cells treated with PEG-HCCs alone resulted in 95% survival ($p = 0.511$), with 100 μM H_2O_2, 62% of the cells survived ($p < 0.0001$), cotreatment with 8 mg/L PEG-HCCs resulted in 94% survival ($p = 0.105$) (Fig. 9B).

To study the toxicity of MB in bEnd.3 cells, cultured cells were treated with 0, 5, 10, and 20 μM MB in PBS cultured overnight, the live cell count indicated a dose-dependent reduction in viability with all concentrations of MB tested having cytotoxic effects on the bEnd.3 cells (Fig. 9C). The concentration of MB was selected based on previous work by May *et al.* on MB reduction in erythrocytes where the authors used a concentration range up to 20 μM MB in packed erythrocytes.[42] These concentrations are also within the mass concentration

(mg/L) range, 4–8 mg/L of PEG-HCCs used in these experiments. A similar assay was performed with MB at 0, 5, 10 and 20 μM given alone or 15 min after initial exposure to 100 μM H_2O_2 (Fig. 9D). In this second challenge assay there was a dose-dependent reduction in cell survival with respect to MB concentration (0–20 μM).

Protection of bEnd.3 Cells from Cyanide Poisoning by PEG-HCCs

If indeed PEG-HCCs are able to influence mitochondria electron transfer, we would predict they would have protective properties against mitochondrial complex poisons, as previously demonstrated with AntA.[4] The effect of PEG-HCCs was tested following acute cyanide poisoning in cultured cells. bEnd.3 cells were treated with 5 mM sodium cyanide (NaCN), a concentration higher than the human LD_{50} reported by Hebert as 2.9 mg/kg (0.874 mM).[43] After treating the cells with NaCN, the cells were then treated with PEG-HCCs at 0, 15, and 30-min after initial poisoning. PEG-HCCs protected the bEnd.3 cells when given immediately following exposure to 5 mM NaCN (83% of PBS-treated bEnd.3 cells vs. 56% in 5 mM NaCN-treated cells, $p = 0.0031$; Fig. 10A). A second experiment was performed to survey the protective effects of PEG-HCCs at 1 mM and 10 mM NaCN. Because of off-gassing, it is likely that the final cyanide concentration is less than the starting concentration.[44] Likewise, the apparent higher cell viability in the 10 mM NaCN T=0 time point also likely due to off-gassing which contributes to experimental variation. Note that increasing concentrations of sodium cyanide reduced cell viability when PEG-HCCs were not added. No reduction in viability occurred when the cells were treated with 1 mM NaCN-treated cells. A time-dependent reduction of protection by PEG-HCCs was noted when cells were treated at 15 and 30 min following initial NaCN exposure for 5 and 10 mM NaCN-treated cells (Fig. 10B). Simultaneous treatment after 10 mM sodium cyanide was protective, but without any further rescue at 15 min (Fig. 10B).

Discussion

In this study we demonstrate that PEG-HCCs catalytically oxidize NADH and ascorbic acid to reduce resazurin and CytC. Our prior work characterizing SOD-mimetic-like activity,[23] and the present findings of additional activity related to mitochondrial-relevant constituents are both consistent with the concept that PEG-HCCs are acting as nanozymes,[13] with therapeutic potential for a range of conditions involving both oxidative stress and mitochondrial electron leakage.

The effects described here are consistent with the broad electrochemical reductions of PEG-HCCs (Fig. 2). In relation to a standard hydrogen electrode the maxima of the PEG-HCC reductions are −1750 and −750 mV, encompassing the reduction potential of NADH of approximately −380 mV. The single electron reduction of semiascorbate to ascorbate at pH 7 is approximately −320 mV versus a standard hydrogen electrode making it comparable to NADH.[45] A principal limitation in the methodology of the cyclic voltammetry measurements was an inability to collect multiple scans due to the solubility of the particles in the PBS buffer used, hence their absence from the figure.

The reduction potential of PEG-HCCs is thought to be an important contributor to the activity of the particles in our reaction conditions. Following the electrochemical gradient,

with NADH having the highest negative reduction potential (−320 mV vs. SHE) and resazurin having the highest positive reduction potential (+380 mV vs. SHE) a material with a reduction potential between the two should act as an intermediate electron acceptor/donor. Indeed, the reduction potential for PEG-HCCs has an onset near 0 V vs. Ag/AgCl, or +280 mV vs. SHE with the peak of the reduction at −750 mV vs. Ag/AgCl, or −460 vs. SHE. On the other hand, as reported by Shirman *et al.*, PEG-PDIs have a reduction potential of −460 mV vs. SCE, or −216 mV vs. SHE.[28] Despite both compounds having reduction potentials between the reduction potential of NADH and resazurin, only PEG-HCCs show any significant catalytic action towards resazurin (Fig. 7). The width of the reduction of PEG-PDIs is smaller than the width of the reduction of PEG-HCCs suggesting that PEG-HCCs may be able to accept electrons from a wider range of potentials compared to PEG-PDIs.[28] Furthermore, there is a notable difference in the physical size of the PEG-PDIs compared to PEG-HCCs. As we reported previously, PEG-HCCs have a core molecular weight of approximately 156,000 Da while the core of PEG-PDIs is only 390 Da.[17, 23, 28] PEG-HCCs may have many more active sites than a PDI molecule so even though there are approximately 400-fold fewer PEG-HCCs than PEG-PDIs in solution at the same mass concentration there may be substantially more reactive sites on the particle. Of principal interest are the availability of quinone residues which are known to be electrochemically active towards NADH.[8, 46] PEG-PDIs are devoid of quinones whereas PEG-HCCs have many quinone sites per particle.[8, 17, 28]

Because both NADH and the resazurin appear to form a ternary complex with the PEG-HCCs, and there likely needs to be sufficient space for the two cofactors to bind. The core of PEG-PDIs are small (approximately 11 × 4 Å in area) and are likely sterically hindered by their large PEG chains limiting the likelihood that the donor-acceptor molecules, NADH and resazurin, respectively will be able to arrive on the surface of the PEG-PDI. PEG-HCCs, despite having much more PEG are also much larger so access to the particle surface may be relatively easier.

In total, despite PEG-PDIs having a suitable reduction potential it may not be wide enough, and the PEG-PDIs may not physically be large enough to accommodate the chemical species studied in these experiments. Additionally, PEG-PDIs may lack essential functional groups that are necessary for the observed reactivity. Notably, PDIs are less effective against the toxic effects of H_2O_2 at comparable carbon concentrations (data not shown), although it is not established that the above differences from the PEG-HCCs explain this difference in efficacy.

In order to better understand the reaction mechanism of PEG-HCCs with NADH we conducted steady-state EPR studies to determine if the PEG-HCCs were undergoing a chemical change. We observed that the steady-state intrinsic radical of the PEG-HCCs is increased by 30–40% (Fig. 5A) when NADH is added and then returns to a baseline intensity when treated with $CytC_{ox}$ or resazurin (Fig. 5B). The initial reduction occurs in a time-dependent fashion when the particles are treated with NADH (Fig. 5C, D). However, the oxidation by $CytC_{ox}$ or resazurin appears to occur very quickly. We surmise that the rate limiting step is the reduction of the particle by NADH as opposed to the oxidation. These findings indicate that the particles are being reduced by NADH and since no additional EPR

resonances are observed suggests that the reduction potential of the reduced PEG-HCCs has changed from its untreated state. NADH is likely donating a hydride to the PEG-HCC as opposed to a single electron reduction as no new peaks are observed as would be the case with an $NADH^{\bullet+}$ radical.[47] The results from this study are counter to the results we previously reported with superoxide, whereupon superoxide is shown to reduce the radical intensity in PEG-HCCs.[12] This difference may be accounted for due to differences in solvent (DMSO vs. KPi buffer), differences in mechanism (hydride transfer vs. electron transfer), and differences in the donor and acceptor species. Further studies are needed to resolve these issues, but in all, this study suggests that PEG-HCCs are not only capable of being reduced by superoxide, but that they can also be reduced by hydride anion as well.

Another detail from these experiments shows that the stoichiometry of NADH to $CytC_{ox}$ in this reaction is 1:2, with NADH appearing to give up two electrons to PEG-HCCs in order to reduce two separate molecules of $CytC_{ox}$. The two-electron donation is supported by Carlson *et al.* who showed that NADH can reduce quinones via a hydride transfer.[48] This shows that PEG-HCCs can not only undergo single electron reductions as in the case of superoxide, but also two-electron reductions as shown here with NADH while still performing single electron reductions of an oxidizer. It also suggests that the electrons derived from NADH are being transferred to $CytC_{ox}$ in a quantitative fashion as opposed to a partial reaction where some electrons from NADH are shunted to dioxygen to form superoxide.

We hypothesized that quinone residues may be responsible for, or modulate the reactivity of PEG-HCCs towards NADH and $CytC_{ox}$ and resazurin. NADH is readily oxidized by various quinones as described by Carlson *et al.* In order to better understand the role of quinones on PEG-HCCs we reacted PEG-HCCs with ethylenediamine.[27] This approach to empirical determination of site function has been demonstrated previously by other authors.[49] The resulting particles, EN-PEG-HCCs, provide evidence that quinone residues are an influencing factor in the reaction between NADH, resazurin, and the PEG-HCCs. Treatment with ethylenediamine effectively eliminating the electrochemical reduction of the particles as indicated by cyclic voltammetry (Figure 6A). Additional studies are needed to address these mechanisms in more detail. It is possible that the quinone sites on their own are not responsible for the reactivity towards NADH itself, but may modulate the activity of nearby sites. One possible mechanism of action is that a hydride is donated to a PEG-HCC by NADH at one carbonyl of a quinone, the resulting adjacent enolate-adjacent carbonyl abstracts a proton from hydronium ion in solution.[48]

In the exploration of the catalytic activity of the PEG-HCCs, we found that the K_M parameter for resazurin in the NADH and Asc oxidation reactions (Tables 2, 3 and 4) were within one order of magnitude of the K_M for the dismutation of superoxide (7.50×10^{-4} M).[23] Because of the closeness of the K_M parameters, we suspect that a common host active site is responsible for the reaction, and as stated earlier, quinone groups are candidates. The k_{cat}, or turnover numbers, for PEG-HCCs are unsurprisingly low considering the V_{max} for the tested concentrations for both NADH and ascorbate-driven reactions. The low k_{cat} parameters may be advantageous in the context of PEG-HCCs influencing electron transfer in mitochondria. Under normal physiological conditions the inclusion of a material that

oxidizes NADH with comparable rates to Complex I would potentially be toxic as it may inhibit the transport of protons into the intermembrane space given that we have no evidence that these materials are also transporting protons, although that needs to be investigated. However, under pathological conditions, it is possible that the kinetics of electron transfer seen here may be sufficient to be protective.

A schematic of potential reaction pathways in mitochondria that our results suggest PEG-HCCs may participate in are shown in Fig. 11. We propose that these actions may include both the quenching of reactive oxygen species, support of electron leakage, and, depending on the electron acceptor, restoration of the mitochondrial membrane potential and reduction of dioxygen to water.

Looking further into the mechanism, the Lineweaver-Burk plots in Fig. 3 show sets of three intersecting lines. The appearance of intersecting lines, while varying the concentration of both reagents, NADH and resazurin, or Asc and resazurin suggest the formation of a ternary complex, or transient complex of all three reagents, as part of the reaction mechanism.[50] The order of the arrival of either reactive species is likely random; however, in order for the reaction to occur, the NADH must first be oxidized by the particle in order to reduce the resazurin or the CytC. Because the substrates are different species, they also likely have different affinities for the particles thus giving a fractional proportion of either species bound to the particle at any given time. Because the reaction rate varied linearly with respect to NADH (Fig. 3B) but non-linearly with respect to resazurin (Fig. 3C), we expect that the affinity for PEG-HCCs is greater for resazurin than for NADH because increasing the concentration of resazurin will saturate the particles over a shorter concentration range (micromolar vs. millimolar increments). In the reaction with Asc and resazurin with PEG-HCCs as the catalyst, the V_{max} is much faster per mole of ascorbate than NADH at all concentrations tested (Table 2 and Table 4). The faster kinetics at the same temperature imply that the reaction mechanism requires a lower activation energy. Again, the Lineweaver-Burk transformation of the saturation curves shown in Fig. 5A show intersecting lines with decreasing slope that depends on the concentration of Asc, indicating a ternary complex likely participates in the catalytic reaction. The reduction of $CytC_{ox}$ by Asc was too fast to properly measure and was thus not included in this study. The reaction between Asc and the PEG-HCCs may be distinct from the reaction between PEG-HCCs and NADH, but we do not yet have a granular understanding of either reaction mechanism and can only speculate. Based on EPR results showing a slow increase in the magnitude of the intrinsic radical after NADH and a rapid decrease after subsequent addition of CytC or resazurin, the oxidation of NADH appears to be the rate limiting step and thus the oxidation of ascorbic acid is likely also rate limiting but much faster. Further details of the mechanism are being pursued.

In the reaction with NADH and $CytC_{ox}$, we see the appearance of a sigmoidal relationship of reaction rate (Fig. 3E) with respect to $CytC_{ox}$ concentration. The sigmoidal shape of the curve suggests a cooperative effect,[50] and the Hill coefficient for the reaction of NADH and $CytC_{ox}$ (Table 3) is greater than 1, supporting a positive cooperative effect.[50] There are at least two scenarios one could imagine for how this process works: protein coronas, or the association of proteins with suspended nanoparticles. Either can show a sigmoidal

relationship for protein association vs concentration.[51] One possible explanation in this case is that as $CytC_{ox}$ molecules bind to the surface of the PEG-HCCs, forming contact sites which another incoming molecule of $CytC_{ox}$ would have a higher affinity for as opposed to a bare, particle surface. A second possibility is that at low concentrations of $CytC_{ox}$ the rate that NADH molecules react with PEG-HCCs carrying $CytC_{ox}$ is relatively low, but as the concentration of $CytC_{ox}$ increases, the likelihood of the reaction occurring increases as well until the reaction rate reaches a maximum velocity related to the oxidation of NADH by the PEG-HCCs.

The sigmoidal relationship of reaction rate to $CytC_{ox}$ also appears in the MB- catalyzed reaction shown in Fig. 9A. We cannot attribute the sigmoidal reaction rate curve to binding to the surface of a particle. In this case it may be that MB binds to $CytC_{ox}$ and undergoes reduction when NADH reduces the MB to leukomethylene blue (LMB).

While there are similarities in reactivity between MB and PEG-HCCs, there are also key differences. MB has been previously demonstrated to have a positive effect on restoring mitochondrial respiration in models of mitochondrial impairment and oxidative stress.[14, 15, 36] Our standard *in vitro* assay of oxidative stress reduction is to co-incubate bEnd.3 cells overnight with 100 μM H_2O_2 and PEG-HCCs.[10] When we performed a H_2O_2 rescue assay with PEG-HCCs and MB we saw two divergent sets of results. PEG-HCCs unequivocally prevented cytotoxicity following H_2O_2 exposure in bEnd.3 cells (Fig. 9B). However, treatment with MB was inherently cytotoxic at all concentrations (Fig. 9C). Treatment of 100 μM H_2O_2-exposed cells with MB resulted in a higher cell death fraction than with only 100 μM H_2O_2 exposure (Fig. 9D). One possible cause of this cytotoxicity is the formation of H_2O_2 following the reduction of MB by NADPH or glutathione to LMB and its subsequent reaction with dioxygen in the cell.[52] The MB effect might be concentration dependent, and lower concentrations may be less toxic and/or protective, but at molar equivalents, the results favor the PEG-HCCs.

The K_Ms for PEG-HCCs in this reaction are within the same order of magnitude as the K_M of PEG-HCCs acting as catalysts in the dismutation of superoxide, 160–87 μM for NADH and resazurin vs. 750 μM for superoxide as reported in our previous work.[23] The k_{cat} parameter is considerably smaller, 0.02–0.06 vs. 20,000 s^{-1} reported for PEG-HCCs with superoxide.[23] This result could suggest that while PEG-HCCs are quite capable of competing with pathological effects of superoxide in-vivo, they would be less able to compete with the targets of NAD(P)H oxidation, such as Complex I under normal conditions. The reported NADPH oxidation turnover number of bovine Complex I, for instance, is > 5000 s^{-1},[53] 5 orders of magnitude greater than the overall turnover number of PEG-HCCs with NADH and resazurin. Under physiological conditions it would likely be detrimental for the particles to have a high turnover number since they would be extracting and shuttling electrons from the endogenous reductant pool in the mitochondria at the expense of reduced proton pumping efficiency and reduced mitochondrial membrane potential. Under a pathological condition, such as a chronic impairment of Complex I or III, PEG-HCCs may be able to provide support to get electrons out of the reductant pool and transport them to higher potential acceptors and either maintain the mitochondrial membrane potential or provide electrons to the oxygen reduction site of Complex IV.

While this mechanism is speculative, it is tentatively supported by ability to protect against mitochondrial complex poisons without evidence of toxicity.[4]

Deconvolution microscopy suggests co-localization of the PEG-HCCs with mitochondria through the visualization of the covalently bound PEG moiety. While it is difficult to say with certainty that the anti-PEG signal was coming from within the mitochondria due to refraction limits, electron microscopy obtained by Huq *et al.* suggest PEG-HCCs internalize in mitochondria.[29] Thus, the internalization of PEG-HCCs in mitochondria does not seem unreasonable. Furthermore, work by Zhang *et al.* showed that Glycyrrhetinic Acid-modified poly(ethylene glycol)-functionalized graphene oxide was capable of colocalizing with mitochondria.[54] The internalization mechanism is not known, however PEGylated graphene and graphene oxides are known to anchor to membranes due to the amphiphilic nature of the particle and PEG.[32] Limitations of fluorescence microscopy at this length scale make it difficult to ascertain the precise location of the PEG-HCCs, but the colocalized signal suggests that an association does exist. The mechanism by which PEG-HCCs localize to membranes is not known, but other work suggests that pegylated graphene oxide, while not an identical material, has an affinity for membranes.[32, 55] The association with mitochondria also seems reasonable from the perspective of charge-charge interactions. The mitochondrial intermembrane space has an overall positive charge,[56] and PEG-HCCs have a slight negative charge so it may be a possible mechanism for access to the mitochondrial inner membrane.[8]

We tested the ability for PEG-HCCs to protect bEnd.3 cells from NaCN, a potent Complex IV inhibitor that binds indiscriminately to heme iron. In the electron transport complex, cyanide binds to oxidized heme a3 with high affinity leading to an interruption of electron transfer and consequently oxidative phosphorylation by preventing the reduction of dioxygen to water. We previously showed that PEG-HCCs protected bEnd.3 cells from AntA,[7] a Complex III inhibitor and conjectured that it may be possible for PEG-HCCs to likewise protect against NaCN poisoning presumably through an electron shuttling mechanism. PEG-HCCs protected the cells when given immediately following exposure to 5 mM NaCN in media (Fig. 10A) and limited protection at later time points. Furthermore, protection from 10 mM NaCN was also achievable when treated with PEG-HCCs immediately following exposure (Fig. 10B). Further direct studies of mitochondria are underway to this mechanism *in vivo*.

MB has been experimentally utilized as an antidote for cyanide poisoning based on its potential as an ETS.[57–59] Cyanide exposure can come from a variety of sources including intentional poisoning or exposure to polyurethane combustion byproducts. Existing antidotes for cyanide exposure include thiosulfates (thiocyanate-generator) nitrites (methemoglobinemia inducer), and hydroxocobalamin (high-affinity cyanide trap). Early large animal *in vivo* experiments by Eddy showed that NaCN reduced respiration rate and salivary gland secretions in 15 kg dogs given at 5 μmol/kg (6.0×10^{-5} M in blood assuming a blood to mass ratio of 85 mL/kg)[60] NaCN.[57] Pre-treatment with 1 mL/kg of 1% MB (3.6×10^{-4} M in blood) 10 min prior to the initial exposure to NaCN reduced the depressive effect of NaCN on respiration and salivary gland excretions. A lethal dose of NaCN in dogs was found to be 3 mg/kg (7.2×10^{-4} M in blood) but could be protected against with 10 mg/kg (3.7×10^{-4} M in blood) MB given either 10 min prior to exposure or 2

min following initial exposure.[57] The concentration of sodium cyanide used by Eddy is nearly the minimum concentration used in our studies and protection by PEG-HCCs is still observed at a concentration over 5-fold higher.

Based on these experiments and the literature, three activity pathways are suggested that provide protection against cyanide poisoning. First, PEG-HCCs may protect the mitochondria by shifting the redox state of CytC to favor more $CytC_{red}$ than normal through an electron shuttling mechanism by capturing electrons from reductants in the intermembrane space, or ubiquinol and transferring them to $CytC_{ox}$. This would in turn lead to an increase in the amount of reduced cytochrome a3 as Complex IV is reduced by $CytC_{red}$. Cyanide has a lower affinity for Fe(II) than it does for Fe(III) and thereby shifting the reduction state of mitochondria to favor more $CytC_{red}$,[59] or reduced Cyt_{a3} may explain some of the protection afforded the cells. This mechanism is opposite of how sodium nitrite functions as an antidote which works by oxidizing hemoglobin in the blood to methemoglobin. Our proposed mechanism forcibly shifts the reduction state of the iron in Cyt_{a3} to favor more ferrous heme than ferric heme thus lowering the affinity of cyanide for Cyt_{a3}.[59] Second, PEG-HCCs may keep the Cyt_{a3} site in a reduced state, by oxidizing NADH and reducing Cyt_{a3} directly, again facilitating electron transfer and reducing the affinity for cyanide on the oxygen reduction portion of the electron transport complex. The third effect is that PEG-HCCs still can function as superoxide dismutase mimetics, thus they may dismutate superoxide generated by Complexes I, II, and III saving the cell from oxidative death but not maintaining the electron transport complex. These pathways do not necessarily need to stand alone and may run in parallel. Further experiments are needed to determine the mechanism of action.

Conclusions

We have provided evidence that PEG-HCCs are able to interact with key mitochondrial constituents in a manner consistent with support of electron transport and acting as nanozymes. If confirmed to occur by the mechanism of catalytic electron transfer in-vivo, this ability, in conjunction with their already established broad antioxidant capacity, suggests new opportunities to address mitochondrial disorders. Features critical to this activity, such as the functional groups and broad redox activity, are under examination and might enable optimization of these materials for treatment of disorders of electron transport.

Experimental Methods

Materials

L-ascorbic acid (Asc, A0278), ferricytochrome c ($CytC_{ox}$, 105%, C2037), methylene blue hydrate (MB, 28514), nicotinamide adenine dinucleotide (NADH, 43420), phosphate buffered saline (PBS, P5368), resazurin sodium salt (R7017–1G), sodium cyanide (NaCN, 97%, 380970) were purchased and used without further purification from Sigma Aldrich (St. Louis, MO). LIVE/DEAD Viability/Cytotoxicity Kit for Mammalian Cells (L3224) was purchased from Thermo-Fisher (Waltham, MA). Poly(ethylene glycol)-functionalized hydrophilic carbon clusters and poly(ethylene glycol)-functionalized perylene diimides were prepared as detailed prevously.[8, 17]

Cyclic Voltammetry

Cyclic voltammograms were obtained on a CHI1202 Electro-Chemical Analyzer (CH Instruments) of a 10 mL sample of PBS buffer solution, pH 7.4 using a three electrode cell. The PEG-HCCs were deposited onto a glassy carbon electrode that was used as the working electrode, while a platinum wire served as a counter electrode and Ag/AgCl served as the reference electrode. CVs were recorded at a scan rate of 200 mV/s, with an initial starting E of 0 mV, high E of +500 mV and low E of −2500 mV.

Electron Paramagnetic Resonance (EPR) Detection of Radicals

EPR measurements of PEG-HCCs containing samples were recorded in a Bruker EMX spectrometer using the following parameters: center field, 3,310 G; sweep width, 100 G; microwave frequency, 9.3 GHz; microwave power, 1 mW; receiver gain, 1.0×10^5; modulation frequency, 100 kHz; modulation amplitude, 1 G; signal channel conversion, 163.8 ms; time constant, 327.7 ms; and sweep time, 167.8 s; temperature 118K. .

Steady-State reaction with NADH

PEG-HCCs samples, 400 or 300 mg/L in KPi buffer, were first premixed with 150 μM of $CytC_{ox}$ (or 150 μM resazurin) in 2 ml Eppendorf tubes at room temperature (23 °C). The reaction was started with addition of 300 μM NADH for ~10 s. During this period the sample was transferred to 5-mm EPR tube and quickly frozen in ethanol/dry ice and then transferred to liquid N_2 to stop the reaction and preserve the intrinsic radical of PEG-HCCs. After the first recording of EPR spectra at 118K, the sample was warmed up in water bath (23 °C) for 1–2 min, frozen in ethanol/dry ice, transferred to liquid N_2 and EPR spectra re-measured. This process was repeated 7 times within 10 min time-frame as indicated in Fig.5 panels C and D.

Spectroscopic Measurement of Catalytic Reduction of Resazurin or Cytochrome c by NADH and Ascorbic Acid and PEG-HCCs

An 8 mM solution of NADH was prepared by dissolving 283 mg of Na_2NADH into 50 mL of PBS. A solution of 8 mM ascorbic acid was prepared by dissolving 146 mg ascorbic acid into 25 mL PBS and titrating the solution with 0.1 M NaOH to pH 7. A stock solution of 2 mM sodium resazurin was prepared by dissolving 25 mg into 50 mL PBS. A stock solution of 500 μM $CytC_{ox}$ was prepared by dissolving 60 mg into 10 mL PBS. Serial dilutions were performed in 1:1 steps from the resazurin and $CytC_{ox}$ stock solutions to make 8-step concentration gradients from 500 μM to 3.9 μM. To a 96-well plate, 25 μL of either resazurin or $CytC_{ox}$ solution was added in triplicate for each concentration gradient step followed by 25 μL of PBS, 25 μL of 16 mg/L PEG-HCCs. The plate was then placed into a plate reader (CLARIOstar, BMG) equipped with an autoinjector. To each well, 25 μL of NADH of 8 mM, 4 mM, or 2 mM was injected automatically. In the case of samples run with ascorbic acid, 1 mM, 0.5 mM, or 0.25 mM was used instead. Following injection, the plate was shaken for 2 s to mix. Each well was read every 4 min for 16 min resulting in a total of five measurements per well using either 570 nm and 600 nm, in the case of resazurin, or 550 nm in the case of $CytC_{ox}$ as the measured wavelength.

To calculate the concentration of resorufin in each well, the following formula was used:

$$[Ruf] = \frac{(34798*A_{570}) - (47619*A_{600})}{(104395*34798) - (47619*5494)}$$

To calculate the concentration of ferrocytochrome C ($CytC_{red}$) in the solution, the absorbance at 550 nm was divided by the extinction coefficient of $CytC_{red}$ at 550 nm, 21.84 mM^{-1} cm^{-1}. Reaction rates were calculated in MARS using linear regressions of concentration vs. time. Michaelis-Menten kinetics parameters and Lineweaver-Burk transformations were calculated by using Prism Graphpad 8.

Stoichiometry of NADH reduction of Cytochrome C

UV-vis measurements were collected using a Hewlett-Packard 8453 UV-vis spectrophotometer of 2.8 mg/L PEG-HCCs with 1 mM NADH and 0.1 mM $CytC_{ox}$ in 50 mM KPi buffer every 10 s. Reaction rates were calculated by subtracting the beginning absorption from the final absorption for 340 nm and 550 nm corresponding to NADH and $CytC_{red}$ respectively. Next, the difference was divided by the extinction coefficients of the two compounds, 6.22 $mM^{-1}cm^{-1}$ for NADH, and 21.84 $mM^{-1}cm^{-1}$for $CytC_{red}$ to give the molar reaction rates for each reagent.

Synthesis of ethylenediamine-blocked PEG-HCCs (EN-PEG-HCCs)

The method was taken from Qi *et al.*[27] An aqueous solution of PEG-HCCs (5.0 mL, 1.2 mg/mL, 6 mg) was added to ethylenediamine (5.0 mL, 4.5 g, 75 mmol). Water was removed via the rotovap, leading to precipitation of the PEG-HCCs in ethylenediamine. MeOH (6 mL) was added, to disperse the PEG-HCCs, along with molecular sieves. The reaction was allowed to stir at room temperature for 5 d before dilution in DI H_2O and filtration by a 0.22 μm polyethersulfone (PES) membrane. The material was purified via crossflow filtration (Spectrum Labs Kros*flo*, Research II*i* TFF System) with a 50 kDa mPES dialysis column (~1 atm transmembrane pressure) to yield 15 mL of EN-PEG-HCC with a carbon core concentration of 400 mg/L.

Protection of bEnd.3 Cells from H_2O_2 by MB and PEG-HCCs

Murine brain endothelioma cells (bEnd.3) suspended in DMEM with 10% FBS and 1% Penicillin-Streptomycin were seeded into 16 wells of one 24-well plate, and two 6-well plates at a density of 40,000 cells/well. Three days later the cells in the 24-well plate were treated in duplicate with either PBS, 5 μM, 10 μM, or 20 μM MB. Another group of cells were treated with 100 μM H_2O_2 alone, or with 5 μM, 10 μM, or 20 μM methylene blue added 15 minutes after initial treatment with 100 μM H_2O_2. In the two six-well plates, two wells were treated with PBS, two with 100 μM H_2O_2, two with 8 mg/L PEG-HCCs, and two with 100 μM H_2O_2 and 8 mg/L PEG-HCCs added immediately after initial exposure. The following morning the cells were detached with trypsin and labeled with calcein-AM and ethidium homodimer and a LIVE/DEAD count was performed.

Immunofluorescence and Imaging

SHSY-5Y cells transfected with mito-PAGFP expressing GFP with a cytochrome c oxidase subunit IV targeting sequence were plated on poly-L-lysine coated glass coverslips and left

overnight to attach.[30] The following morning, the cells were treated with 8 mg/L PEG-HCCs for 30 min. Cells were fixed in 4% paraformaldehyde for 20 min on ice, quenched with 0.1M ammonium chloride for 15 min and permeabilized with 0.1% Triton-X100 for 20 min at room temperature. After 1 hour of blocking in 5% milk/TBST, cells were incubated overnight at 4 °C with anti-polyethylene glycol [PEG-B-47] rabbit monoclonal antibody (Abcam, ab51257, USA). The cells were washed with blocking buffer (5% milk/TBST), incubated with AlexaFluor647-conjugated anti-rabbit antibody (1/1000, ThermoFisher, OR, USA) in blocking buffer for 1 hour at room temperature, and counterstained with DAPI (1 μg/ml). The samples were imaged using a DeltaVision (GE Healthcare, USA) image restoration deconvolution microscope with an Olympus 100X U PlanS-Apo/1.4 NA oil immersion lens. Z-stacks were obtained with an interplane distance of 0.25 μm.

Colocalization of PEG-HCCs in bEnd.3 Cells

The Z-stacks obtained from deconvolution microscopy were processed using the FIJI (FIJI is Just ImageJ) distribution of ImageJ.[37] Briefly, the channels in each Z-stack were separated and the AlexaFluor 647 and GFP channels were binarized using the Otsu thresholding algorithm. Next, a coincidence layer was constructed from the binary AND mask of the AlexaFluor 647 and GFP channels at each layer within the Z-stack. Finally, the DAPI, AlexaFluor 647, and the binary coincidence AlexaFluor 647 - GFP channels were composited and a Z-projection was performed.

Treatment of bEnd3 Cells from Sodium Cyanide

DANGER: Sodium cyanide is poisonous at olfactorily detectable concentrations! Immediate symptoms include shortness of breath, blue coloration of fingernails and lightheadedness. If these symptoms appear, immediately alert others in the area, isolate the area, relocate to fresh air and contact emergency services. Murine cortical endothelioma cells (bEnd.3) suspended in DMEM with 10% FBS and 1% PCN-STM were seeded into a 24-well cell culture tray at a concentration of 50,000 cells/well and left to incubate for two days at 37 °C under 5% CO_2. Following incubation, 10 mL of a 50 mM solution of sodium cyanide was prepared by dissolving 24.5 mg into 10 mL PBS in a chemical fume hood. Solutions of 1, 5, and 10 mM NaCN in media were prepared by diluting 150 μL, 1500 μL, or 3000 μL of NaCN-containing PBS to 14.85 mL, 13.5 mL, and 12.0 mL of complete media respectively. Afterwards, and PEG-HCCs were given at a concentration of 8 mg/L at 0, 15, and 30 min to each set. A separate negative control (PBS) and positive control (cyanide, no PEG-HCCs) were included. The cells were then returned to the incubator for 24 h.

Viability Assays of CN^--treated bEnd.3 Cells

The following day, the media in each well was removed and the cells were rinsed twice with 1 mL of PBS. The cells were detached using 1 mL of trypsin and vigorous pipetting. The contents of each well were transferred to 1.7 mL Eppendorf tubes and 500 μL of complete DMEM media and the cell suspensions were centrifuged at 1300 RPM for 10 min. Following centrifugation, the media was removed by vacuum, replaced with 1 mL of complete media, and the cells were resuspended by pipette and brief vortex mixing. A LIVE/DEAD (Calcein-AM/Ethidium homodimer, Invitrogen) assay was performed by first

diluting 8 μL of Calcein-AM and 2 μL of Ethidium homodimer stock solutions into 8 mL of complete media.

Supplementary Material

Refer to Web version on PubMed Central for supplementary material.

Acknowledgements

We thank Drs Michael A. Mancini (email mancini@bcm.edu) and Fabio Stossi (stossi@bcm.edu) of the Baylor College of Integrated Microscopy Core for assistance with deconvolution microscopy.

Funding Sources

Supported by NIH grants R21NS084290 and R01NS094535 (MPIs: TK, JT, and A-LT). TAK was supported by grant number BE-0048 from the Robert A. Welch foundation. PJD was partially supported by the National Heart, Lung, and Blood Institute of the National Institutes of Health under award number T32HL007747. KM was partially supported by the Department of Defense National Defense Science Engineering Graduate (NDSEG) Fellowship. The content is solely the responsibility of the authors and does not necessarily represent the official views of the National Institutes of Health. The contents do not represent the views of the U.S. Department of Veterans Affairs or the United States Government. Imaging for this project was supported by the Integrated Microscopy Core at Baylor College of Medicine with funding from NIH (DK56338, and CA125123), CPRIT (RP150578, RP170719), the Dan L. Duncan Comprehensive Cancer Center, and the John S. Dunn Gulf Coast Consortium for Chemical Genomics.

References

1. Segal BH, Grimm MJ, Khan AN, Han W and Blackwell TS, Free Radic Biol Med, 2012, 53, 72–80. [PubMed: 22583699]
2. Brieger K, Schiavone S, Miller FJ Jr. and Krause KH, Swiss Med Wkly, 2012, 142, w13659. [PubMed: 22903797]
3. Nour M, Scalzo F and Liebeskind DS, Intervent Neurol, 2013, 1, 185–199.
4. Bitner BR, Marcano DC, Berlin JM, Fabian RH, Cherian L, Culver JC, Dickinson ME, Robertson CS, Pautler RG, Kent TA and Tour JM, ACS Nano, 2012, 6, 8007–8014. [PubMed: 22866916]
5. Zweier JL and Talukder MA, Cardiovasc Res, 2006, 70, 181–190. [PubMed: 16580655]
6. Quinlan CL, Orr AL, Perevoshchikova IV, Treberg JR, Ackrell BA and Brand MD, J Biol Chem, 2012, 287, 27255–27264. [PubMed: 22689576]
7. Marcano DC, Bitner BR, Berlin JM, Jarjour J, Lee JM, Jacob A, Fabian RH, Kent TA and Tour JM, J Neurotrauma, 2013, 30, 789–796. [PubMed: 22928502]
8. Berlin JM, Leonard AD, Pham TT, Sano D, Marcano DC, Yan S, Fiorentino S, Milas ZL, Kosynkin DV, Price BK, Lucente-Schultz RM, Wen X, Raso MG, Craig SL, Tran HT, Myers JN and Tour JM, ACS Nano, 2010, 4, 4621–4636. [PubMed: 20681596]
9. Berlin JM, Pham TT, Sano D, Mohamedali KA, Marcano DC, Myers JN and Tour JM, ACS Nano, 2011, 5, 6643–6650. [PubMed: 21736358]
10. Fabian RH, Derry PJ, Rea HC, Dalmeida WV, Nilewski LG, Sikkema WKA, Mandava P, Tsai AL, Mendoza K, Berka V, Tour JM and Kent TA, Front Neurol, 2018, 9, 199. [PubMed: 29686642]
11. Samuel EL, Duong MT, Bitner BR, Marcano DC, Tour JM and Kent TA, Trends Biotechnol, 2014, 32, 501–505. [PubMed: 25175886]
12. Jalilov AS, Zhang C, Samuel EL, Sikkema WK, Wu G, Berka V, Kent TA, Tsai AL and Tour JM, ACS Appl Mater Inter, 2016, 8, 15086–15092.
13. Wu J, Wang X, Wang Q, Lou Z, Li S, Zhu Y, Qin L, Wei H; Chem. Soc. Rev 2019, 48, 1004–1076 [PubMed: 30534770]
14. Atamna H, Nguyen A, Schultz C, Boyle K, Newberry J, Kato H and Ames BN, FASEB J, 2008, 22, 703–712. [PubMed: 17928358]

15. Lee KK, Imaizumi N, Chamberland SR, Alder NN and Boelsterli UA, Hepatology, 2015, 61, 326–336. [PubMed: 25142022]
16. Salaris SC, Babbs CF and Voorhees WD, Biochem Pharmacol, 1991, 42, 499–506. [PubMed: 1650213]
17. Jalilov AS, Nilewski LG, Berka V, Zhang C, Yakovenko AA, Wu G, Kent TA, Tsai AL and Tour JM, ACS Nano, 2017, 11, 2024–2032. [PubMed: 28112896]
18. Purich DL, in Enzyme Kinetics: Catalysis & Control, Elsevier, 2010, ch. 6.
19. Purich DL, in Enzyme Kinetics: Catalysis and Control, Elsevier, 2010, ch. 11.
20. Copeland RA, Enzymes: A Practical Introduction to Structure, Mechanism, and Data Analysis, Wiley-VCH, 2nd edn., 2000.
21. Software G, GraphPad Curve Fitting Guide Equation: Allosteric sigmoidal, https://www.graphpad.com/guides/prism/7/curve-fitting/index.htm?reg_allosteric_enzyme.htm, (accessed 11/01/2018, 2018).
22. Li X, Cobb CE, Hill KE, Burk RF and May JM, Arch Biochem Biophys, 2001, 387, 143–153. [PubMed: 11368176]
23. Samuel EL, Marcano DC, Berka V, Bitner BR, Wu G, Potter A, Fabian RH, Pautler RG, Kent TA, Tsai AL and Tour JM, Proc Natl Acad Sci U S A, 2015, 112, 2343–2348. [PubMed: 25675492]
24. Roessler MM and Salvadori E, Chem Soc Rev, 2018, 47, 2534–2553. [PubMed: 29498718]
25. Bernofsky C and Wanda S-YC, J. Biol. Chem, 1982, 257, 6809–6817. [PubMed: 7045095]
26. Hayashi T, Asano Y, Shintani Y, Aoyama H, Kioka H, Tsukamoto O, Hikita M, Shinzawa-Itoh K, Takafuji K, Higo S, Kato H, Yamazaki S, Matsuoka K, Nakano A, Asanuma H, Asakura M, Minamino T, Goto Y, Ogura T, Kitakaze M, Komuro I, Sakata Y, Tsukihara T, Yoshikawa S and Takashima S, Proc Natl Acad Sci U S A, 2015, 112, 1553–1558. [PubMed: 25605899]
27. Carlson BW; Miller LL; Mechanism of the oxidation of NADH by quinones. Energetics of one-electron and hydride routes. J. Am. Chem. Soc 1985, 107(2), 479–485.
28. Shirman E, Ustinov A, Ben-Shitrit N, Weissman H, Iron MA, Cohen R and Rybtchinski B, J Phys Chem B, 2008, 112, 8855–8858. [PubMed: 18597517]
29. Huq R, Samuel EL, Sikkema WK, Nilewski LG, Lee T, Tanner MR, Khan FS, Porter PC, Tajhya RB, Patel RS, Inoue T, Pautler RG, Corry DB, Tour JM and Beeton C, Sci Rep, 2016, 6, 33808. [PubMed: 27654170]
30. Karbowski M, Cleland MM and Roelofs BA, Methods Enzymol, 2014, 547, 57–73. [PubMed: 25416352]
31. Bobadilla AD, Samuel EL, Tour JM and Seminario JM, J Phys Chem B, 2013, 117, 343–354. [PubMed: 23206183]
32. Chen J, Zhou G, Chen L, Wang Y, Wang X and Zeng S, J Phys Chem C, 2016, 120, 6225–6231.
33. Dixon SJ, Lemberg KM, Lamprecht MR, Skouta R, Zaitsev EM, Gleason CE, Patel DN, Bauer AJ, Cantley AM, Yang WS, Morrison BI and Stockwell BR, Cell, 2012, 149, 1060–1072. [PubMed: 22632970]
34. Latunde-Dada GO, Biochim Biophys Acta, 2017, 1861, 1893–1900.
35. Ashurst J and Wasson M, Del Med J, 2011, 83, 203–208. [PubMed: 21954509]
36. Lee KK and Boelsterli UA, Redox Biol, 2014, 2, 599–609. [PubMed: 25460728]
37. Visarius TM, Stucki JW and Lauterburg BH, FEBS Lett, 1997, 412, 157–160. [PubMed: 9257711]
38. Florence TM, J Inorg Biochem, 1984, 22, 221–230.
39. Coyle CH, Martinez LJ, Coleman MC, Spitz DR, Weintraub NL and Kader KN, Free Radic Biol Med, 2006, 40, 2206–2213. [PubMed: 16785034]
40. Nulton-Persson AC and Szweda LI, J Biol Chem, 2001, 276, 23357–23361. [PubMed: 11283020]
41. Winterbourn CC, Toxicol Lett, 1995, 82/83, 969–974. [PubMed: 8597169]
42. May JM, Qu ZC and Cobb CE, Am J Physiol Cell Physiol, 2004, 286, C1390–1398. [PubMed: 14973146]
43. Hebert CD, NTP Technical Report on Toxicity Studies of Sodium Cyanide, 1993.
44. Arun P, Moffett JR, Ives JA, Todorov TI, Centeno JA, Namboodiri MA and Jonas WB, Anal Biochem, 2005, 339, 282–289. [PubMed: 15797569]

45. Sapper H, Kang S-O, Paul H-H and Lohmann W, Z. Naturforsch, 1982, 37, 942–946.
46. Céas NK, Kanapienienė JJ and Kulys JJ, Biochimica et Biophysica Acta, 1984, 767, 108–112. [PubMed: 6487613]
47. Zielonka J, Marcinek A, Adamus J and Gębicki J, The Journal of Physical Chemistry A, 2003, 107, 9860–9864.
48. Carlson BW and Miller LL, J Am Chem Soc, 1985, 107, 479–485.
49. Sun H, Zhao A, Gao N, Li K, Ren J and Qu X, Angew Chem Int Ed Engl, 2015, 54, 7176–7180. [PubMed: 25940927]
50. Segel IH, Enzyme Kinetics: Behavior and analysis of rapid equilibrium and steady-state enzyme systems, Wiley-Interscience, United States of America, 1993.
51. Vilanova O, Mittag JJ, Kelly PM, Milani S, Dawson KA, Radler JO and Franzese G, ACS Nano, 2016, 10, 10842–10850. [PubMed: 28024351]
52. Kelner MJ and Alexander NM, The Journal of Biological Chemistry, 1985, 260, 15168–15171. [PubMed: 4066667]
53. Fedor JG, Jones AJY, Di Luca A, Kaila VRI and Hirst J, Proc Natl Acad Sci U S A, 2017, 114, 12737–12742. [PubMed: 29133414]
54. Zhang C, Liu Z, Zheng Y, Geng Y, Han C, Shi Y, Sun H, Zhang C, Chen Y, Zhang L, Guo Q, Yang L, Zhou X and Kong L, Small, 2018, 14, 1703306
55. Luo N, Weber JK, Wang S, Luan B, Yue H, Xi X, Du J, Yang Z, Wei W, Zhou R and Ma G, Nat Commun, 2017, 8, 14537. [PubMed: 28233871]
56. Frantz MC and Wipf P, Environ Mol Mutagen, 2010, 51, 462–475. [PubMed: 20175113]
57. Eddy NB, Journal of Pharmacology and Experimental Therapeutics, 1931, 41, 449–464.
58. Judenherc-Haouzi A, Zhang XQ, Sonobe T, Song J, Rannals MD, Wang J, Tubbs N, Cheung JY and Haouzi P, Am J Physiol Regul Integr Comp Physiol, 2016, 310, R1030–1044. [PubMed: 26962024]
59. Beasley DM and Glass WI, Occup Med (Lond), 1998, 48, 427–431. [PubMed: 10024740]
60. Diehl K-H, Hull R, Morton D, Pfister R, Rabemampianina Y, Smith D, Vidal J-M and van de Vorstenbosch C, Journal of Applied Toxicology, 2001, 21, 15–23. [PubMed: 11180276]

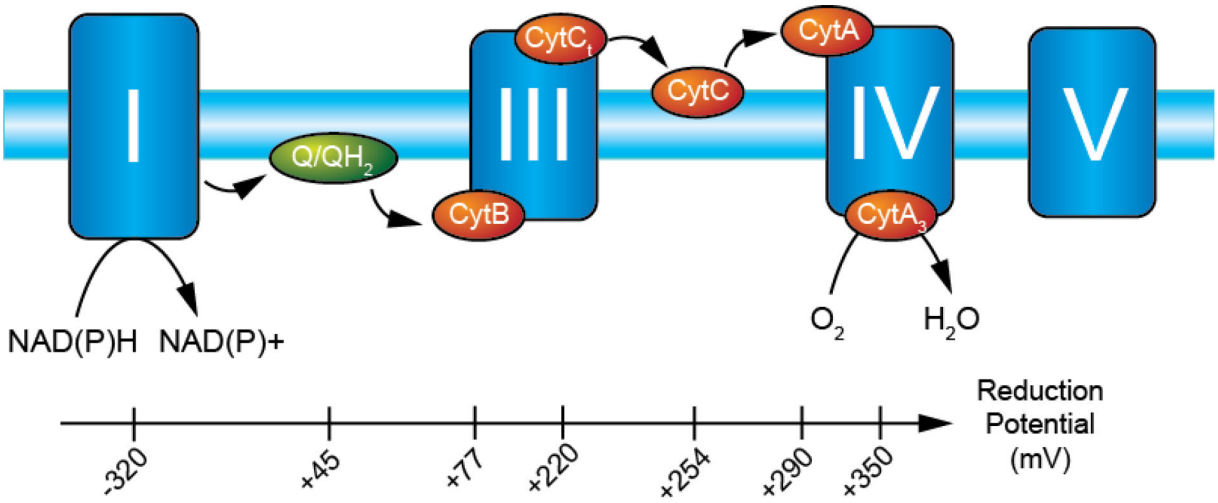

Figure 1.

Reduction potentials of electron transport complex showing the favorable energetics leading to the reduction of dioxygen to water. Each member is reduced in series following the oxidation of NAD(P)H by the flavin moiety in Complex I (−320 mV). The energetics of the electron transport complex are favorable to maintain the proton gradient, the electron carrier (ubiquinone) between Complexes I/II and III, that are spatially separated from the carrier (CytC) between Complexes III and IV. Each reduction/oxidation reaction in Complexes I, III, and IV is used to transport protons from the matrix to the intermembrane space. Proton translocation cross the membrane is coupled with the catalysis of ATP formation by Complex V. Complex II is absent for clarity but reduces ubiquinone at the expense of succinate.

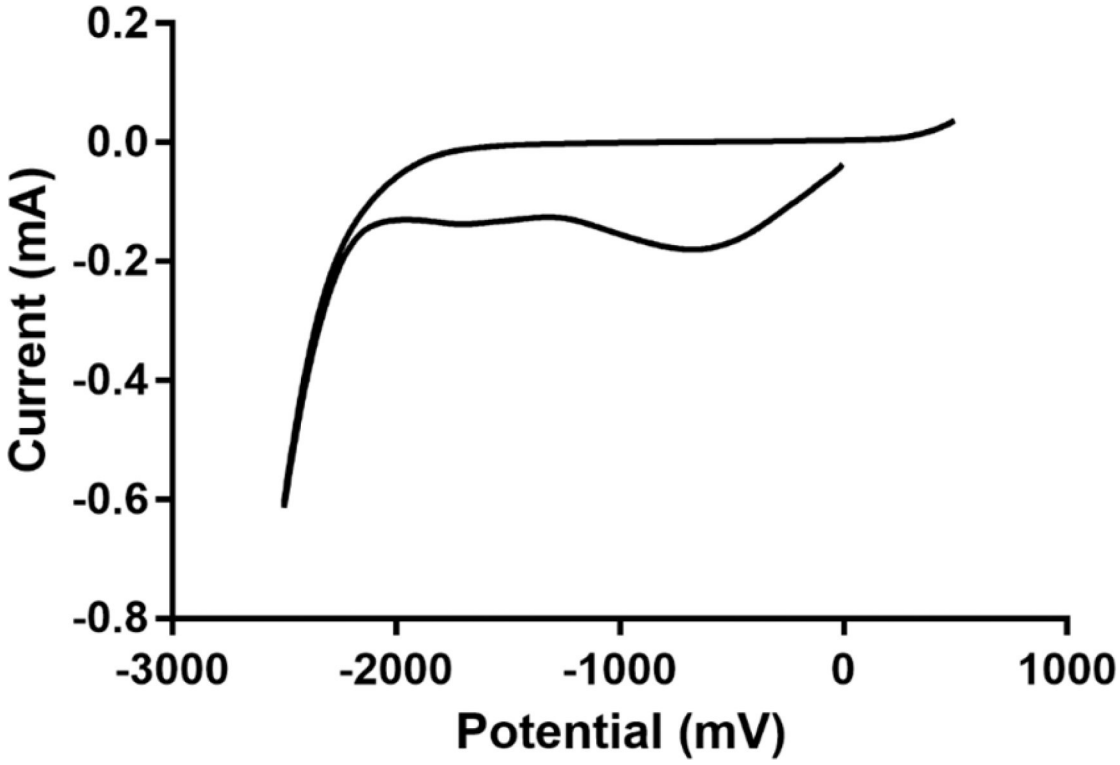

Figure 2.

Cyclic voltammogram of PEG-HCCs in PBS. PEG-HCCs have characteristically broad reduction maxima near −750 mV and −1750 mV as part of a wave beginning at +200 mV and extending to −2 V. Scanning here began from 0 V to −2500 mV.

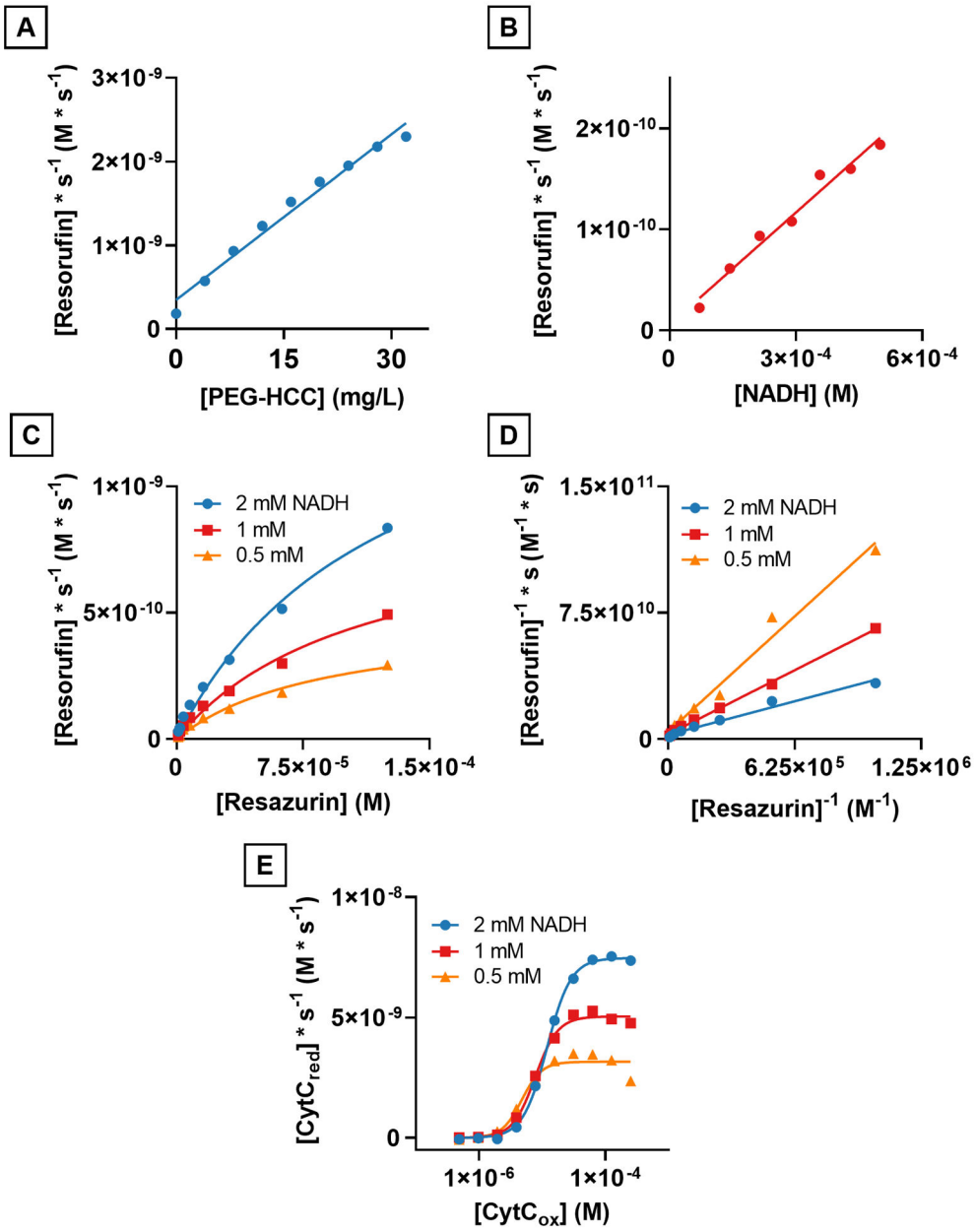

Figure 3.

PEG-HCCs catalytically reduce both resazurin and ferricytochrome c ($CytC_{ox}$) with NADH to resorufin and ferrocytochrome c ($CytC_{red}$), respectively. **A)** The reduction rate of resazurin in the presence of NADH is linearly related to the concentration of PEG-HCCs. **B)** The reduction rate of resazurin while holding the concentration of resazurin and PEG-HCCs constant varies linearly with the concentration of NADH. **C)** The reaction rates of NADH with resazurin and PEG-HCCs is not linearly related to the concentration of resazurin and no saturation point is observed within the detection limits of our instrumentation. **D)** Lineweaver-Burk plot of **C** showing intersecting lines suggesting the role of a ternary complex in the reduction of resazurin. **E)** NADH-linked reduction of $CytC_{ox}$ to $CytC_{red}$ showing a saturation point at all three concentrations of NADH and full sigmoidal curve.

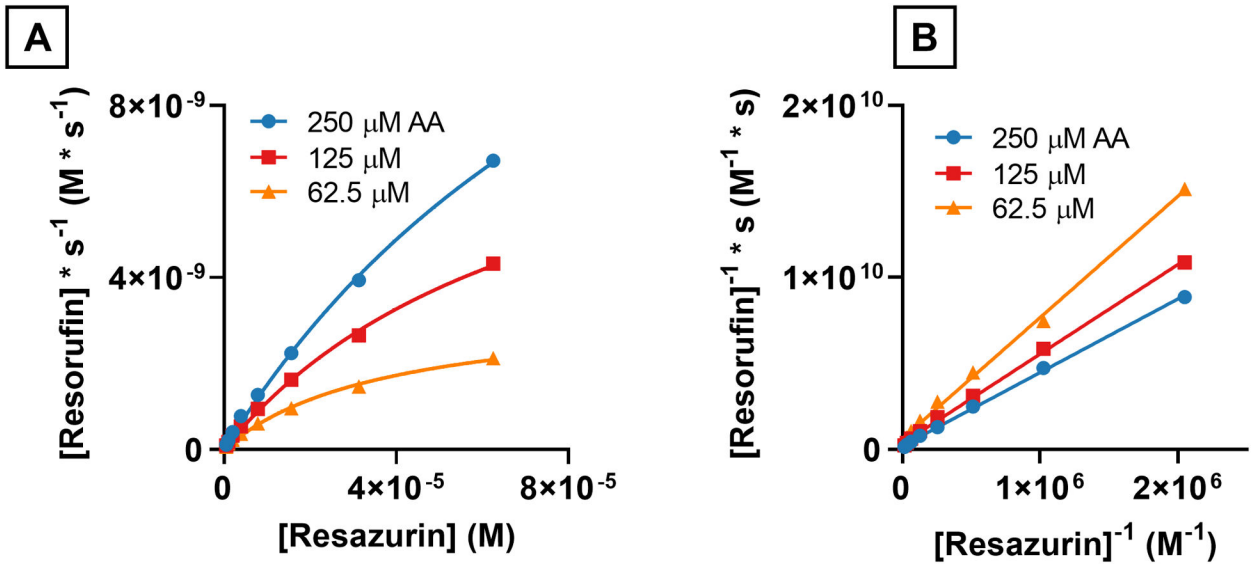

Figure 4.

Reaction rates of ascorbic acid with resazurin and PEG-HCCs at various concentrations of ascorbic acid and resazurin. **A)** Reduction rates of resazurin by ascorbic acid catalyzed by PEG-HCCs (4 mg/L) fit to Michaelis-Menten saturation curves. **B)** Lineweaver-Burk plots of the reaction between resazurin, Asc and PEG-HCCs showing intersecting lines suggesting a ternary complex.

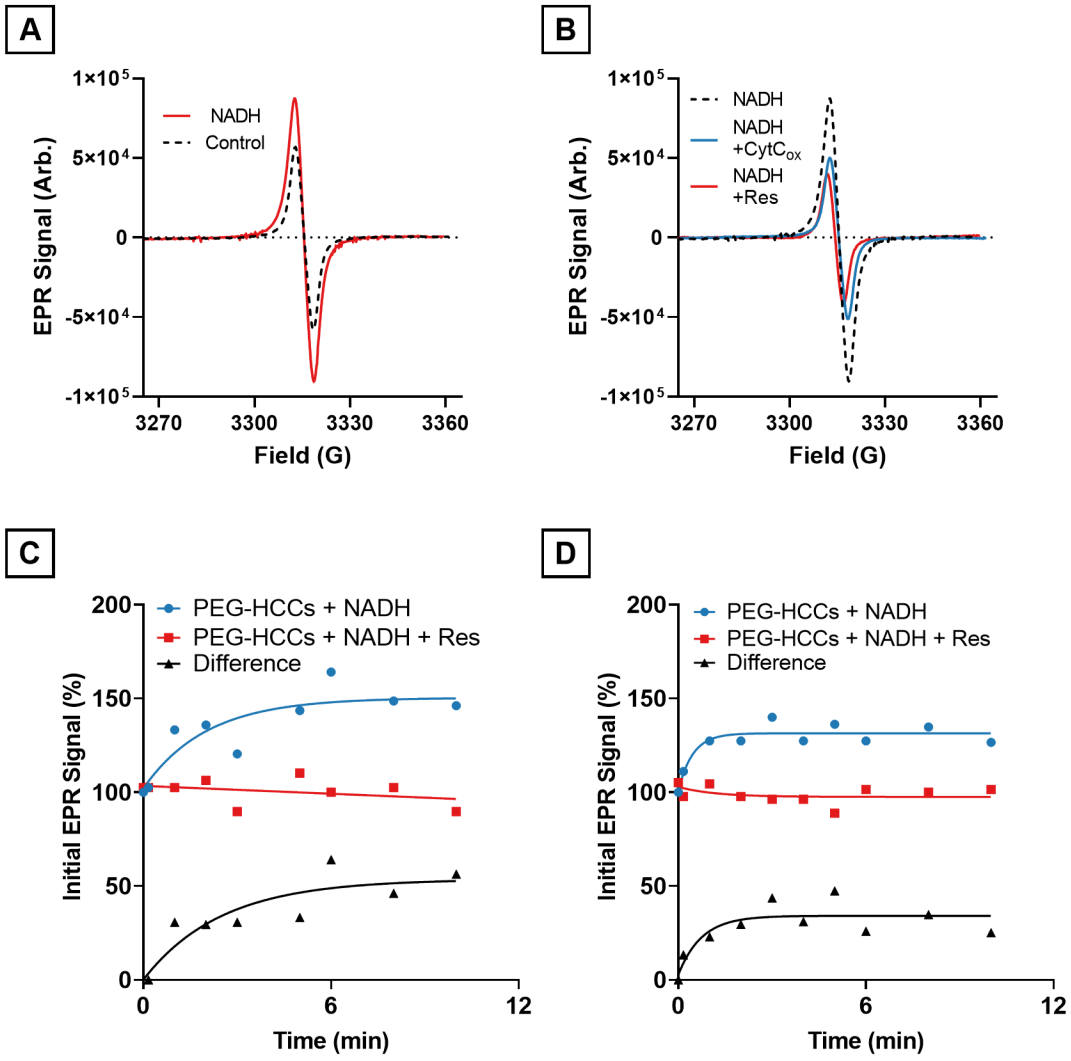

Figure 5.

Electron paramagnetic resonance spectrometry (EPR) of PEG-HCCs in the presence of NADH and ferricytochrome c or resazurin. A) PEG-HCCs exposed to NADH (solid line) for 10 min compared to PEG-HCCs without NADH (black dotted line). B) PEG-HCCs exposed to NADH for 10 min (black dotted line) followed by the addition of ferricytochrome c (CytC, blue line) or resazurin (Res, red line) and flash frozen 10 s later. The resulting EPR signals are slightly lower than the baseline intensity shown in (A). C) Time course plot of PEG-HCC reduction with NADH and its oxidation with Res. The difference in signal intensity between PEG-HCCs treated with only NADH and PEG-HCCs treated with NADH and Res is shown in black. D) Time course plot of PEG-HCC reduction with NADH and its oxidation with CytC. The difference in signal intensity between PEG-HCCs treated with only NADH and PEG-HCCs treated with NADH and CytC is shown in black.

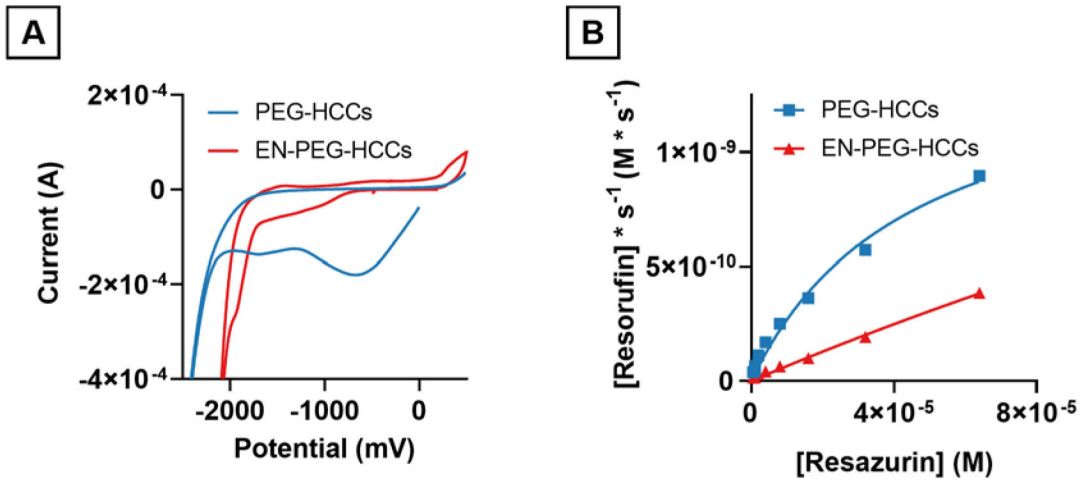

Figure 6.

Cyclic voltammogram and reaction rates of PEG-HCCs and EN-PEG-HCCs. A) Cyclic voltammogram showing PEG-HCCs and EN-PEG-HCCs. EN-PEG-HCCs are absent the strong reduction at −750 mV and −1750 mV but have a new shoulder at approximately −1500 mV. B) Resazurin reduction kinetics. EN-PEG-HCCs reduce resazurin markedly slower than PEG-HCCs at the same concentration of catalyst (4 mg/L).

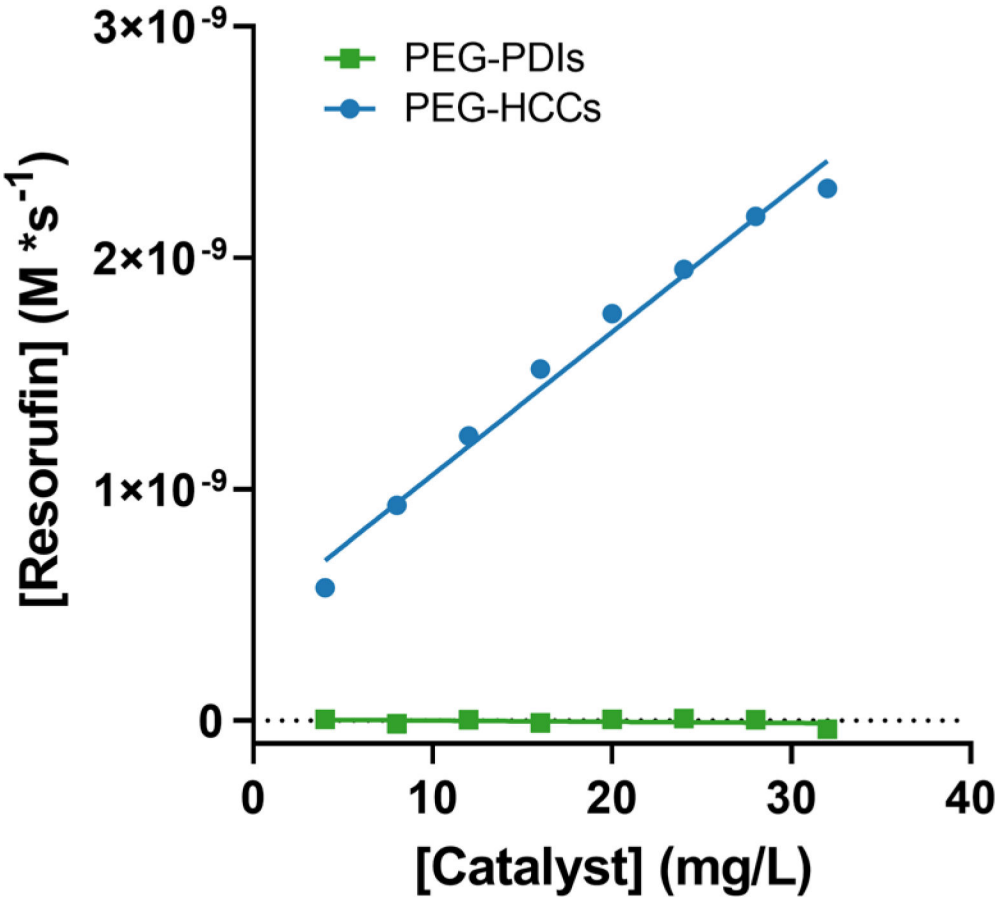

Figure 7.

Reaction rates of PEG-HCCs and PEG-PDIs (4 mg/L – 32 mg/L) with 0.5 mM NADH and 64 μM resazurin. The reaction rate of PEG-PDIs is effectively zero M/s while the reaction rate with PEG-HCCs increases linearly with catalyst concentration.

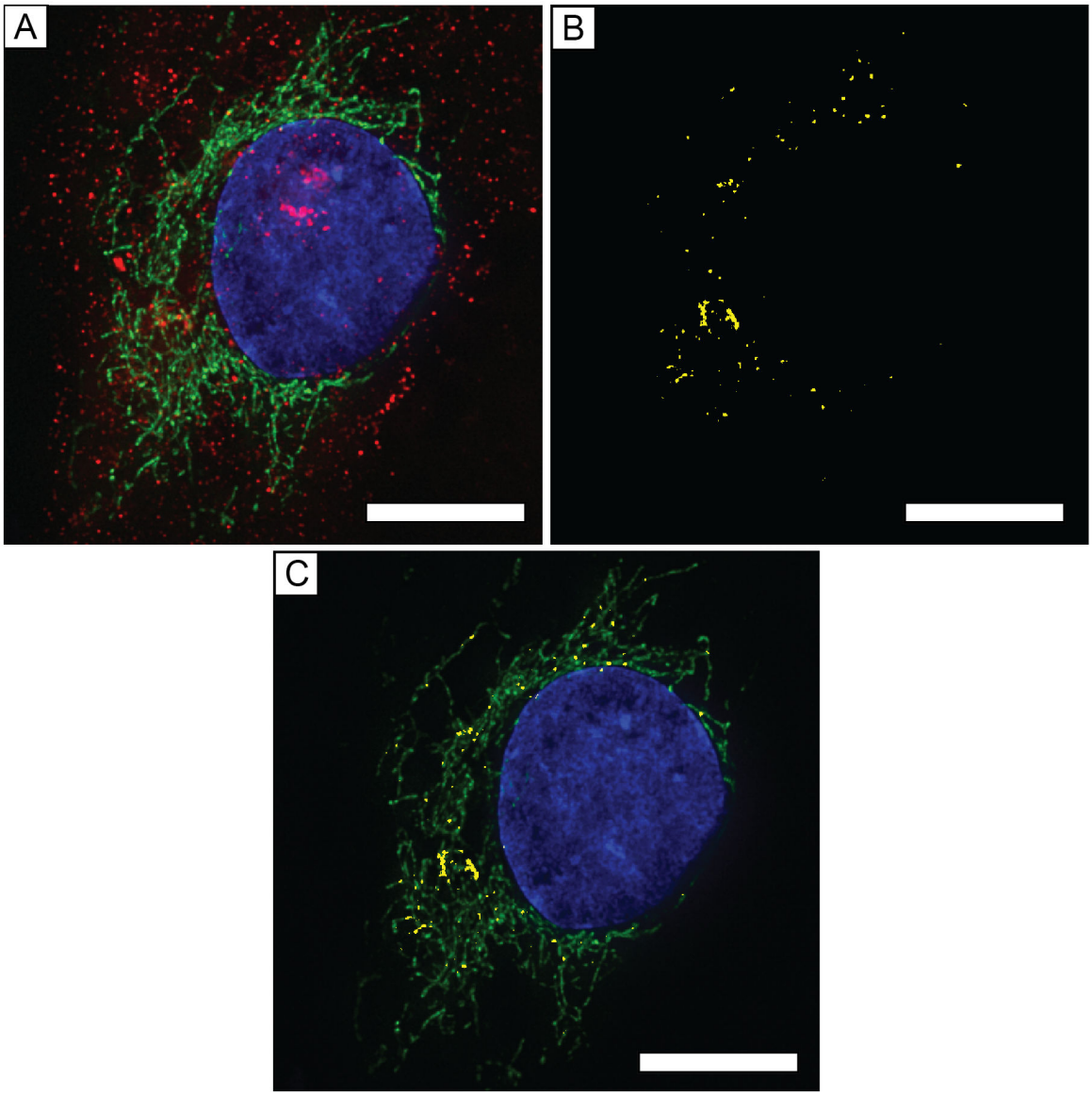

Figure 8.

Deconvolution microscopy images of a bEnd.3 cell treated with PEG-HCCs for 5 min. Nucleus is labeled with DAPI (blue), mitochondria were labeled with GFP containing a CytC oxidase subunit IV targeting sequence (green), and PEG-HCCs were labeled with rabbit-AntiPEG with a secondary AlexaFluor 647-labeled anti-rabbit IgG (red). **A)** Z-projection of SHSY-5Y cell with mitochondria, nucleus, and PEG-HCCs labeled. **B)** Z-projection of ANDed binarized Z-stacks of GFP and AlexaFluor 647 signals. **C)** Composite Z-projection of AlexaFluor 647-GFP and DAPI. Scale bars are all 10 μm.

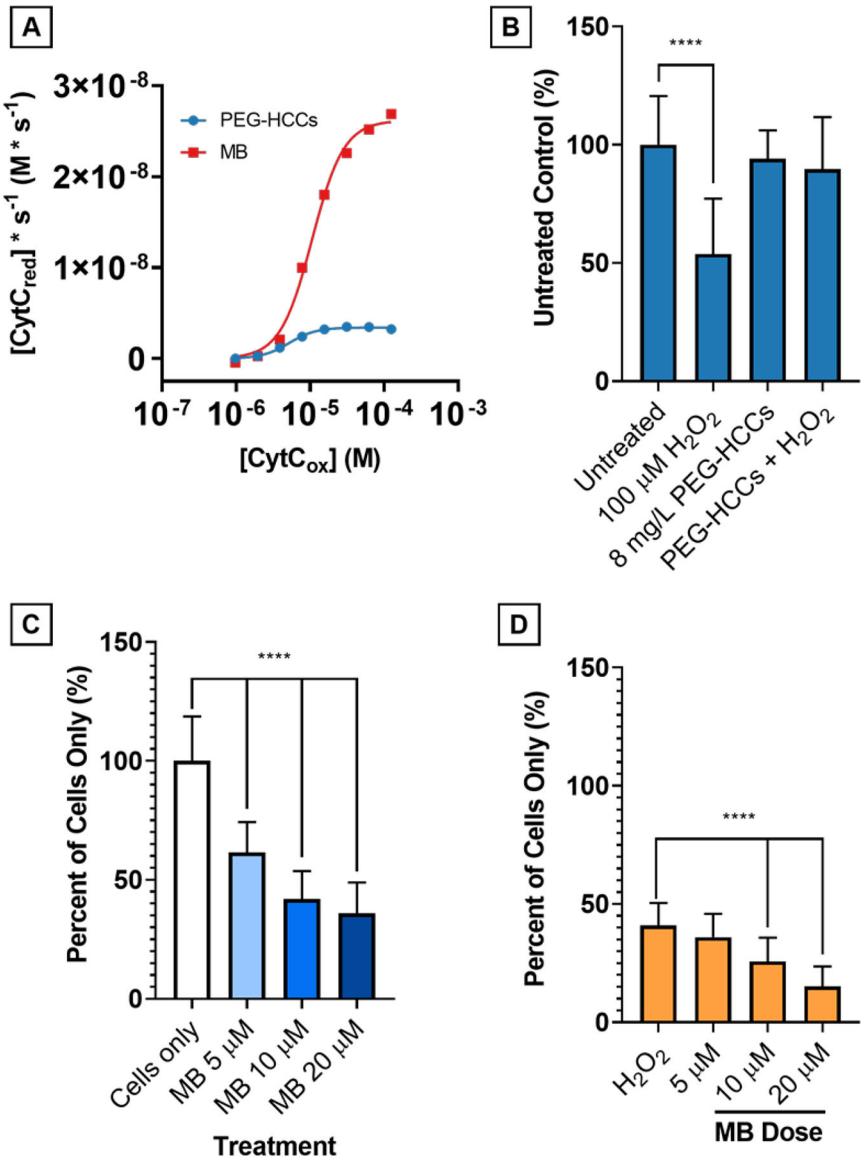

Figure 9.

Comparison of PEG-HCCs and MB at 4 mg/L concentration on reduction of $CytC_{ox}$ by NADH (500 μM). **A)** On a mass concentration basis, MB has a higher V_{max} than PEG-HCCs by nearly one order of magnitude. Without NADH, neither PEG-HCCs nor MB reduce CytC. PEG-HCCs rescue bEnd.3 cells from H_2O_2toxicity while MB is intrinsically toxic. **B)** bEnd.3 cells were treated with 100 μM H_2O_2 (54%, $p < 0.0001$) and 8 mg/L PEG-HCCs were added at 15 minutes following the initial insult. Live cell counts (n = 32) were performed and no toxicity of the PEG-HCCs (94%, $p = 0.511$) is observed, and 8 mg/L PEG-HCCs protection of bEnd.3 cells against H_2O_2 (90%, $p = 0.105$). **C)** MB given at 5, 10, and 20 μM causes dose-dependent cytotoxicity in bEnd.3 cells ($p < 0.0001$ at all levels). **D)** No protection is afforded when given immediately following treatment with 100 μM H_2O_2 ($p < 0.0001$ at all levels except 5 μM, $p = 0.409$).

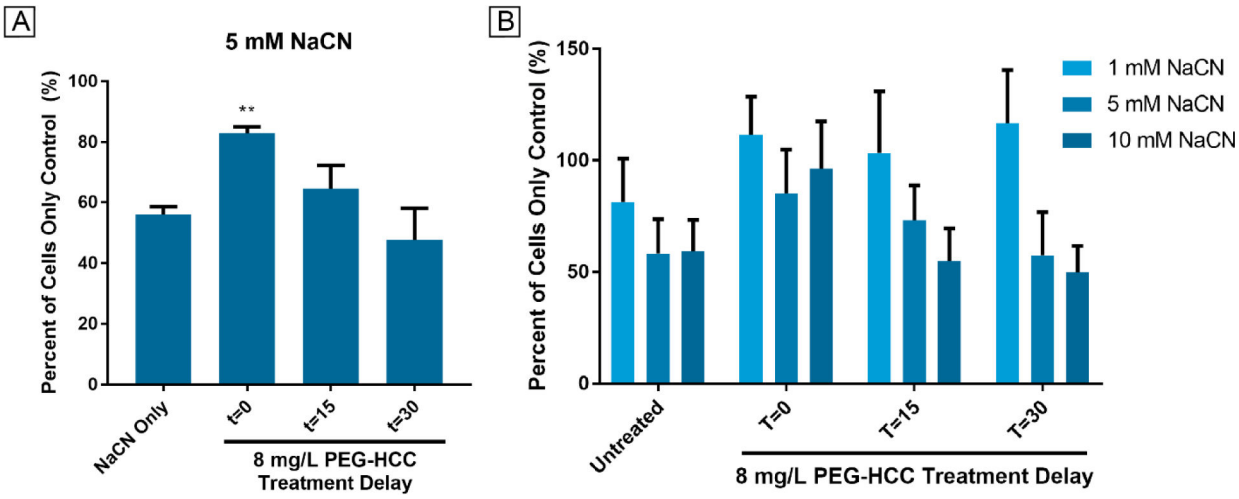

Figure 10.

Effect of cyanide concentration and PEG-HCC administration time on LIVE cell count of bEnd3 cells. **A)** Triplicate experiments with 5 mM NaCN show that PEG-HCCs can significantly (** p = 0.003) reduce death in bEnd.3 cells when given immediately and trends with time to less effectiveness. Averages generated by counting live cells in duplicate wells 16 times. Significance calculated with a Dunnett-corrected one-way ANOVA. **B)** A survey experiment with 1, 5 and 10 mM NaCN showed that PEG-HCCs appear to protect bEnd.3 cells from 1 mM NaCN at 0, 15, and 30 min and afforded partial protection from 5 mM NaCN at 0 and 15 min. Partial protection was also provided by PEG-HCCs when given at 0 min against 10 mM NaCN. All results are relative to untreated negative controls. Positive controls were treated with sodium cyanide at 1, 5, and 10 mM but not PEG-HCCs. The results show an inverse time-dependent and dose-dependent effect. As administration delay increases, the rescue effect is reduced. Error bars show standard deviation of 32 cell counts.

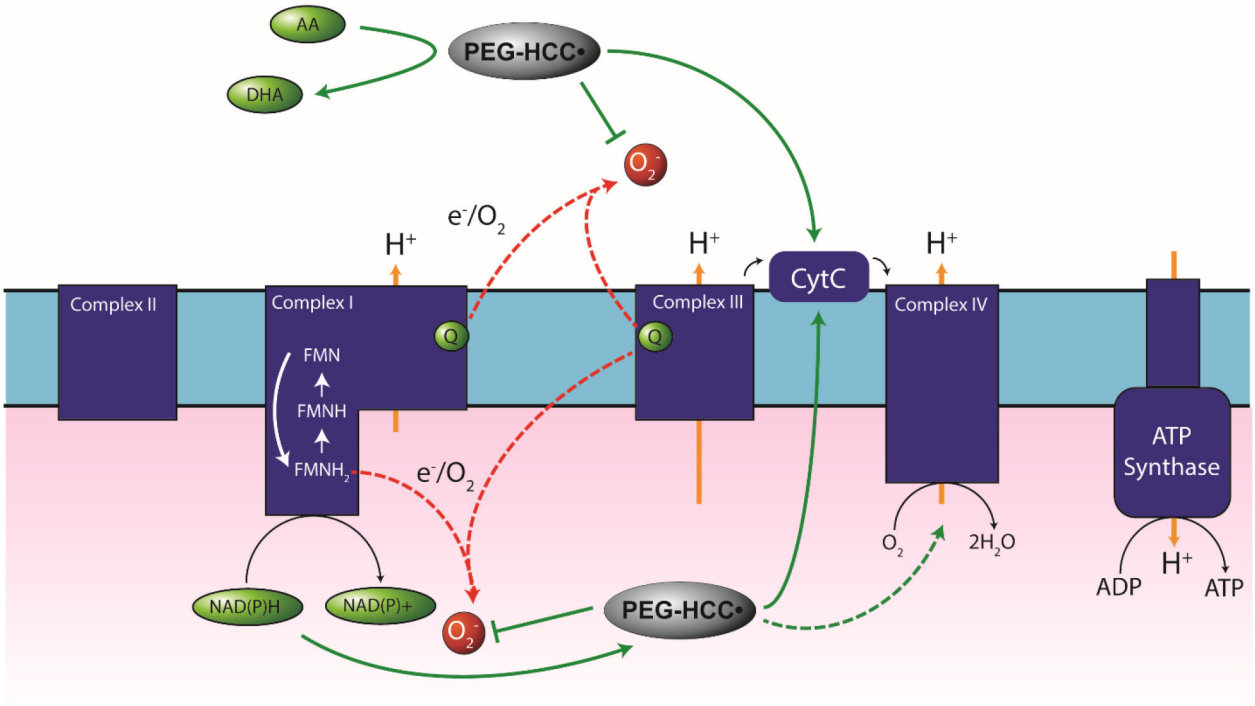

Figure 11. Proposed electron transfer pathways for PEG-HCCs.

PEG-HCCs are reduced by NAD(P)H and Asc and can donate electrons to superoxide, CytC, or potentially the oxygen reduction site Cyt_{a3} on Complex IV. Transferring electrons to CytC from NADH would bypass inhibited Complexes I and III. Transferring electrons from NAD(P)H to Cyt_{a3} would bypass impairment of Complexes I, III, and IV while providing electrons to reduce dioxygen to water. Red dashed arrows: example of electron leakage sites. Green dashed arrow: potential bypassing effects of cyanide. Green solid arrows: potential electron transfer pathways.

Table 1.

Kinetic Parameters for the reduction of resazurin by NADH in the presence of PEG-HCCs. The particle concentration used in these experiments was 4 mg/L (25.6 nM).

	NADH Concentration		
	2 mM	**1 mM**	**0.5 mM**
V_{max} ($M * s^{-1}$)	1.6×10^{-9}	9.1×10^{-10}	4.8×10^{-10}
K_M (M)	1.2×10^{-4}	1.1×10^{-4}	8.7×10^{-5}
k_{cat} (s^{-1})	0.06	0.04	0.02
k_{cat}/K_M ($M^{-1}s^{-1}$)	500	340	230

Table 2.

Kinetics parameters of PEG-HCCs with NADH and $CytC_{ox}$. The particle concentration used in these experiments was 4 mg/L (25.6 nM).

	NADH Concentration		
	2 mM	**1 mM**	**0.5 mM**
V_{max} ($M * s^{-1}$)	7.5×10^{-9}	5.0×10^{-9}	3.2×10^{-9}
h	2.3	2.4	2.8
K_{half} (M)	1.2×10^{-5}	7.7×10^{-6}	4.8×10^{-6}
k_{cat} (s^{-1}) (V_{max}/K_{half})	0.23	0.15	0.09
k_{cat}/K_{half} ($M^{-1} * s^{-1}$)	1.9×10^{4}	1.9×10^{4}	1.94×10^{4}

Table 3.

Kinetic parameters for the reduction of resazurin by ascorbic acid in the presence of PEG-HCCs.

	Asc Concentration		
	250 μM	**125 μM**	**63 μM**
V_{max} (M * s^{-1})	1.93×10^{-8}	9.52×10^{-9}	3.35×10^{-9}
K_M (M)	1.2×10^{-4}	7.6×10^{-5}	3.8×10^{-5}
k_{cat} (s^{-1})	0.75	0.37	0.13
k_{cat}/K_M	6,250	4,870	3,240
V_{max}/[Asc] (s^{-1})	7.7×10^{-5}	7.6×10^{-5}	5.3×10^{-5}

Table 4.

Kinetic parameters for the reduction of $CytC_{ox}$ by NADH in the presence of MB.

	Catalyst	
	4 mg/L MB	**4 mg/L PEG-HCCs**
V_{max} ($M \times s^{-1}$)	20.22×10^{-9}	2.4×10^{-9}
H	2.39	2.8
K_{half} (M)	5.21×10^{-6}	4.8×10^{-6}
k_{cat} (s^{-1}) (V_{max}/K_{half})	1.62×10^{-3}	9.30×10^{-2}
k_{cat}/K_{half} ($M^{-1} \times s^{-1}$)	310	19,400
V_{max}/[NADH] (s^{-1})	4.0×10^{-5}	4.8×10^{-6}